THE GEOLOGICAL SOCIETY OF AMERICA®

Geochronology and geochemistry of Permian to Early Triassic granitoids in the Alxa Terrane: Constraints on the final closure of the Paleo-Asian Ocean

Qian Liu[1], Guochun Zhao[1,2,*], Yigui Han[1], Paul R. Eizenhöfer[3], Yanlin Zhu[1], Wenzhu Hou[1], Xiaoran Zhang[4], and Bo Wang[1]
[1]DEPARTMENT OF EARTH SCIENCES, THE UNIVERSITY OF HONG KONG, POKFULAM ROAD, HONG KONG, CHINA
[2]DEPARTMENT OF GEOLOGY, NORTHWEST UNIVERSITY, XI'AN 710069, CHINA
[3]DEPARTMENT OF GEOLOGY AND PLANETARY SCIENCE, UNIVERSITY OF PITTSBURGH, 4107 O'HARA STREET, PITTSBURGH, PENNSYLVANIA 15260-3332, USA
[4]INSTITUTE OF EARTH SCIENCES, ACADEMIA SINICA, TAIPEI 11529, TAIWAN

ABSTRACT

As a pivotal junction between the North China and Tarim cratons, the Alxa Terrane provides an ideal window to constrain the final closure of the middle segment of the Paleo-Asian Ocean (PAO). This study carried out petrological, whole-rock geochemical, and zircon U-Pb-Hf isotopic investigations on four major granitic plutonic complexes in the Alxa Terrane. The Bayan Nuru and Yabulai plutonic complexes are I-type granitoids that yield crystallization ages of 281–268 Ma and 277–270 Ma, respectively, with negative zircon $\varepsilon_{Hf}(t)$ values (–11.5 to –3.2), primarily sourced from the Neoproterozoic rocks in the region. The Nuergai granitoids yield crystallization ages of 281–268 Ma and show I-type affinities and positive zircon $\varepsilon_{Hf}(t)$ values (+1.6 to +6.4), indicating an origin related to magma mixing. Emplaced at ca. 241 Ma, the Oliji granitoids display varying zircon $\varepsilon_{Hf}(t)$ values from –0.9 to +11.5, which necessitate a predominant source of mantle-derived materials. A compilation of zircon $\varepsilon_{Hf}(t)$ and whole-rock $\varepsilon_{Nd}(t)$ values of the magmatic rocks in the Alxa Terrane illustrates a decreasing trend from the Late Carboniferous to the Early Permian and an increasing trend during Middle Permian to Triassic time. The marked shift with a large variation of zircon $\varepsilon_{Hf}(t)$ and whole-rock $\varepsilon_{Nd}(t)$ values at 280–265 Ma indicates a tectonic switch from subduction to post-collision tectonic regimes in the Alxa Terrane, marking the final closure of the middle segment of the PAO. Comparable isotope variations are also identified from 260 to 245 Ma magmatic counterparts on the northern margin of the North China Craton, hence suggesting a progressively eastward closure of the PAO.

LITHOSPHERE; v. 9; no. 4; p. 665–680; GSA Data Repository Item 2017237 | Published online 25 May 2017 https://doi.org/10.1130/L646.1

INTRODUCTION

As one of the most magnificent orogens in Earth's history, the Central Asian Orogenic Belt (CAOB) formed from the accretion and amalgamation of the Siberia and East Europe cratons to the north and the North China and Tarim cratons to the south, due to multiple episodes of subduction and closure of the Paleo-Asian Ocean (PAO) (Şengör et al., 1993; Khain et al., 2003; Xiao et al., 2003, 2009, 2013, 2015; Jahn, 2004; Windley et al., 2007; Schulmann and Paterson, 2011; Wilhem et al., 2012; Eizenhöfer et al., 2014; Han et al., 2016a, 2016b; Chen et al., 2017). In the past decade, considerable progress has been made in understanding the final closure of the PAO along the Tianshan and Solonker suture zones, which were adjacent to the northern margins of the Tarim and North China cratons (Şengör et al., 1993; Xiao et al., 2003, 2009, 2013, 2015; Windley et al., 2007; Wilhem et al., 2012; Eizenhöfer et al., 2014; Han et al., 2016b). However, controversy still exists regarding the timing of the final closure of the PAO, with different perspectives arguing for distinct closure times that range from the Late Devonian to the Late Triassic (Xiao et al., 2003, 2009, 2013, 2015; Charvet et al., 2007, 2011; Windley et al., 2007; Jian et al., 2008, 2010; Han et al., 2011, 2016b; Wilhem et al., 2012; Xu et al., 2013; Eizenhöfer et al., 2014, 2015a, 2015b; Zhang et al., 2015a, 2015b, 2016a, 2016b).

*Corresponding author: gzhao@hkucc.hku.hk

Located between the North China Craton (NNC) to the east and the Tarim Craton to the west (Fig. 1A), the Alxa Terrane in westernmost Inner Mongolia occupies a crucial place to understand the closure processes in the middle segment of the PAO. The terrane is characterized by large volumes of late Paleozoic to early Mesozoic magmatic rocks, of which the changes of magma sources and isotopic records with time can provide important information for unraveling the history of the consumption of the middle segment of the PAO. In this study, we carried out field-based petrological, zircon U-Pb-Hf isotopic and whole-rock major- and trace-elemental investigations on a variety of Permian to Early Triassic granitoids across the Alxa Terrane. By integrating the new results and previous data, we aim to better constrain the origin of the magmatic rocks, the regional tectonic settings, and the timing of the final closure of the PAO.

GEOLOGICAL BACKGROUND

Located in westernmost Inner Mongolia, the Alxa Terrane is a triangular block separated from the NCC to the east by the Langshan fault (Fig. 1B). The Alxa Terrane borders the North Qilian Orogen to the southwest by the Longshoushan fault and the southernmost CAOB to the north by the Enger Us fault (Fig. 1B). The ca. 300 Ma Enger Us ophiolitic mélange along the Enger Us fault is considered to demarcate the final closure site of the PAO (BGMRIM, 1991; Wang et al., 1994; Wu et al., 1998; Xie et

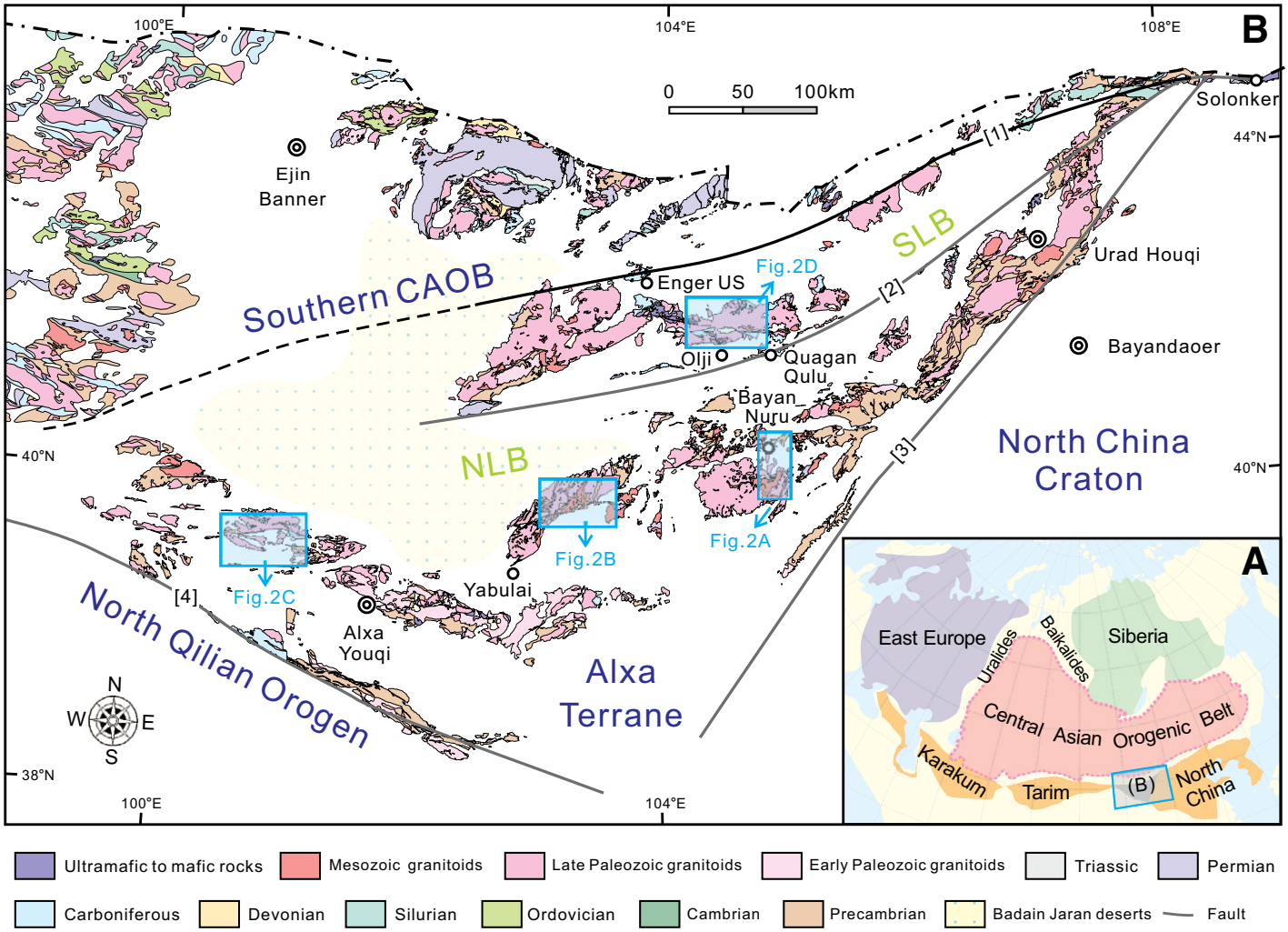

Figure 1. (A) Simplified tectonic sketch map of the Central Asian Orogenic Belt (CAOB) with the location of the Alxa Terrane (modified after Xiao et al., 2013, Han et al., 2016a, 2016b) and (B) Geological map of the Alxa Terrane (modified after 1:200,000 geological maps from Bureau of Geology and Mineral Resources of Inner Mongolia Autonomous Region (1991) and geological map of Tianshan and its adjacent area, 1:1,000,000). [1]—the Enger Us fault; [2]—the Badain Jaran fault; [3]—the Langshan fault; [4]—the Longshoushan fault. SLB—the Shalazhashan belt; NLB—the Nuru-Langshan belt.

al., 2014; Zheng et al., 2014). Largely covered by the Badain Jaran desert, the Alxa Terrane is subdivided into the Nuru-Langshan and Shalazhashan belts separated by the Badain Jaran fault, along which ca. 275 Ma Quagan Qulu ophiolitic mélange outcrops (Fig. 1B) (BGMRIM, 1991; Wang et al., 1994; Wu et al., 1998; Zheng et al., 2014).

Precambrian basement rocks and Paleozoic to Mesozoic magmatic rocks widely occur in the Nuru-Langshan belt (NLB). The Precambrian basements in the belt are composed mainly of ca. 2.5 Ga tonalite-trondhjemite-granodiorite, 2.3–2.0 Ga orthogneisses reworked by high amphibolite-facies metamorphism at 1.93–1.80 Ga, Paleoproterozoic paragneisses, and 970–800 Ma magmatic and sedimentary rocks (Geng et al., 2002; Li et al., 2004; Peng et al., 2010; Geng and Zhou, 2011; Dan et al., 2012, 2014b; Gong et al., 2012; J.X. Zhang et al., 2013; Hu et al., 2014; Wu et al., 2014; Zhao et al., 2015). Voluminous late Paleozoic to early Mesozoic magmatic rocks across the NLB yielded zircon U-Pb ages of 418–239 Ma, with a main peak at the Permian time (summarized in Liu et al., 2016). In addition, some early Paleozoic dioritic and granitic intrusions with zircon ages of 460–423 Ma have been reported in the eastern and southern parts of the NLB (Dan et al., 2015a; Liu et al., 2016).

The Shalazhashan belt (SLB) is composed mainly of late Paleozoic to early Mesozoic magmatic rocks, with subordinate late Paleozoic sedimentary rocks and minor early Paleozoic magmatic rocks and Precambrian basement rocks (Fig. 1B). The late Paleozoic to early Mesozoic magmatic rocks in the SLB include predominant 301–247 Ma granitoids and subordinate 264–249 Ma diorites and gabbros (Ran et al., 2012; W. Zhang et al., 2013; Shi et al., 2014a, 2014b; Yang et al., 2014). The late Paleozoic sedimentary successions are represented by the Amushan Formation, which has Late Carboniferous to Early Permian depositional ages. The lower and middle sequences of the Amushan Formation consist mainly of clastic rocks interbedded with mafic to felsic volcanic rocks that yielded zircon U-Pb ages of 320–302 Ma, and the upper sequence is a molasse composed of silty shale, sandstone, gravel-bearing sandstone, and conglomerate (Lu et al., 2012; W. Zhang et al., 2013).

SAMPLING

In this study, granitic intrusions in the Alxa Terrane were widely sampled, with 17 samples from the eastern to western parts of the NLB and

nine samples from the middle part of the SLB. Due to the paucity of the outcrops in the Alxa Terrane, the contact relationship between different rock types in the same plutonic complex can hardly be recognized in the field. Detailed locations, lithology, mineral assemblages, and analytical results of samples are summarized in Table 1.

The Bayan Nuru Plutonic Complex

Samples 14LQ01A–14LQ01C, 14LQ14A, and 14LQ14B were collected near the Bayan Nuru area in the eastern part of the NLB (Fig. 2A). Intruding the Precambrian basement rocks and intruded by Early Triassic granitoids, the Bayan Nuru granitic plutonic complex contains ultramafic to intermediate intrusive enclosures occurring as small elliptical or irregular bodies (Fig. 2A). These intrusions show crystallization ages varying from 440 Ma to 270 Ma (Fig. 2A; Liu et al., 2016).

Samples 14LQ01A–14LQ01C are monzogranite with a porphyritic texture (Fig. 3A), of which alkali feldspar grains are coarse-grained phenocrysts, and quartz grains mostly appear as fine-grained aggregates showing late recrystallization. Samples 14LQ14A and 14LQ14B are syenogranite, containing more abundance of alkali feldspar with 1% anhedral muscovite and minor minerals of epidote-zoisite and fluorite.

The Yabulai Plutonic Complex

In the middle part of the NLB, four samples (14LQ34A, 14LQ34B, 14LQ35A, and 14LQ35B) were collected from the Yabulai granodioritic plutonic complex, which is intruded by Triassic granitoids in the region (Figs. 2B and 3B). The common minerals are hornblende, biotite, quartz (38%–45%), alkali feldspar (15%–17%), and plagioclase (35%–45%) (Fig. 3C), with minor epidote-zoisite and sphene. Hornblende and biotite grains show preferred orientations yielding a lineation and a gneissosity, respectively (Figs. 3B and 3C). Quartz grains occasionally tend to be tiny grains with undulatory extinction due to ductile shear deformation (Fig. 3C).

The Nuergai Plutonic Complex

Approximately 80 km northwest to Alxa Youqi County (Fig. 1B), the Nuergai granitic plutonic complex in the western part of the NLB is

TABLE 1. SUMMARY OF THE SAMPLING LOCALITY, LITHOLOGY, MINERAL ASSEMBLAGES, AND ANALYTICAL RESULTS

Sample number	Latitude (°N)	Longitude (°E)	Lithology	Mineral assemblages*	Ages (Ma)†	$\varepsilon_{Hf}(t)$§	T^{C}_{DM} (Ga)#
Bayan Nuru plutonic complex, eastern Nuru–Langshan belt							
14LQ01A	39°53'50.0"	105°00'41.5"	Monzogranite	Qtz 36%, Afs 30%, Pl 30%, Hbl 2%, Bt 2%, Ep-Zo	268	–6.1 to –3.2	1.67–1.49
14LQ01B	39°53'50.0"	105°00'41.5"	Monzogranite	Qtz 35%, Afs 25%, Pl 35%, Hbl 2%, Bt 3%, Ep-Zo			
14LQ01C	39°53'50.0"	105°00'41.5"	Monzogranite	Qtz 32%, Afs 25%, Pl 40%, Hbl 1%, Bt 2%, Ep-Zo			
14LQ14A	40°11'14.6"	104°48'24.4"	Syenogranite	Qtz 40%, Afs 40%, Pl 19%, Mus 1%, Ep-Zo, Fl	281	–11.5 to –9.5	2.01–1.90
14LQ14B	40°11'14.6"	104°48'24.4"	Syenogranite	Qtz 40%, Afs 39%, Pl 20%, Mus 1%, Ep-Zo, Fl			
Yabulai plutonic complex, middle Nuru–Langshan belt							
14LQ34A	39°43'22.2"	103°07'57.5"	Granodiorite	Qtz 40%, Afs 15%, Pl 37%, Hbl 3%, Bt 5%, Ep-Zo, Sph	277	–5.1 to –3.0	1.63–1.49
14LQ34B	39°43'22.2"	103°07'57.5"	Granodiorite	Qtz 45%, Afs 17%, Pl 35%, Hbl 1%, Bt 2%, Ep-Zo, Sph			
14LQ35A	39°53'40.4"	103°34'25.6"	Granodiorite	Qtz 40%, Afs 15%, Pl 40%, Hbl 1%, Bt 4%, Ep-Zo, Sph	270	–7.4 to –6.1	1.75–1.64
14LQ35B	39°53'40.4"	103°34'25.6"	Granodiorite	Qtz 38%, Afs 10%, Pl 45%, Hbl 2%, Bt 5%, Ep-Zo, Sph			
Nuergai plutonic complex, western Nuru–Langshan belt							
14LQ26A	39°28'28.3"	101°03'58.9"	Quartz diorite	Qtz 15%, Pl 55%, Hbl 22%, Bt 8%, Ep-Zo, Ap	269	+1.6 to +3.3	1.18–1.08
14LQ26B	39°28'28.3"	101°03'58.9"	Quartz diorite	Qtz 20%, Pl 54%, Hbl 18%, Bt 8%, Ep-Zo, Ap			
14LQ26C	39°28'28.3"	101°03'58.9"	Quartz diorite	Qtz 10%, Pl 50%, Hbl 18%, Bt 22%, Ep-Zo, Ap			
14LQ30A	39°35'03.3"	100°48'37.7"	Syenogranite	Qtz 38%, Afs 52%, Pl 9%, Bt 1%, Ep-Zo, Ap	268	+4.3 to +6.4	1.02–0.89
14LQ30B	39°35'03.3"	100°48'37.7"	Syenogranite	Qtz 40%, Afs 50%, Pl 9%, Bt 1%, Ep-Zo, Ap			
14LQ31A	39°36'22.0"	100°40'19.5"	Syenogranite	Qtz 38%, Afs 55%, Pl 15%, Hbl 1%, Bt 1%, Ep-Zo, Ap	269	+2.6 to +5.3	1.12–0.95
14LQ33A	39°39'01.6"	100°35'06.0"	Granodiorite	Qtz 30%, Afs 15%, Pl 40%, Hbl 10%, Bt 5%, Ep-Zo, Ap, Sph	281	+1.6 to +3.8	1.20–1.06
14LQ33B	39°39'01.6"	100°35'06.0"	Granodiorite	Qtz 28%, Afs 12%, Pl 40%, Hbl 15%, Bt 5%, Ep-Zo, Ap, Sph			
Oliji plutonic complex, middle Shalazhashan belt							
14LQ37A	40°48'53.2"	104°28'19.3"	Granodiorite	Qtz 30%, Afs 10%, Pl 50%, Hbl 5%, Bt 5%, Ep-Zo, Ap, Sph			
14LQ37B	40°48'53.2"	104°28'19.3"	Granodiorite	Qtz 28%, Afs 12%, Pl 50%, Hbl 4%, Bt 6%, Ep-Zo, Ap, Sph			
14LQ38A	40°50'01.2"	104°28'24.5"	Granodiorite	Qtz 30%, Afs 15%, Pl 47%, Hbl 3%, Bt 5%, Ep-Zo, Ap, Sph	241	+8.2 to +11.5	0.75–0.54
14LQ38B	40°50'01.2"	104°28'24.5"	Granodiorite	Qtz 30%, Afs 20%, Pl 40%, Hbl 4%, Bt 6%, Ep-Zo, Ap, Sph			
14LQ39A	40°50'39.7"	104°27'38.4"	Granodiorite	Qtz 28%, Afs 15%, Pl 42%, Hbl 5%, Bt 10%, Ep-Zo, Ap, Sph			
14LQ44A	40°55'01.0"	104°21'04.1"	Monzogranite	Qtz 35%, Afs 33%, Pl 30%, Bt 2%, Ep-Zo, Ap	242	–0.8 to +7.4	1.32–0.80
14LQ44B	40°55'01.0"	104°21'04.1"	Monzogranite	Qtz 40%, Afs 37%, Pl 32%, Bt 1%, Ep-Zo, Ap			
14LQ45A	40°56'18.2"	104°19'32.4"	Monzogranite	Qtz 40%, Afs 35%, Pl 24%, Bt 1%, Ep-Zo, Ap			
14LQ45B	40°56'18.2"	104°19'32.4"	Monzogranite	Qtz 40%, Afs 37%, Pl 22%, Bt 1%, Ep-Zo, Ap			

*Qtz—quartz, Afs—alkali feldspar, Pl—plagioclase, Hbl—hornblende, Bt—biotite, Ep—epidote, Zo—zoisite, Mus—muscovite, Fl—fluorite, Sph—sphene, Ap—apatite.
†Measured zircon U-Pb ages in this study.
§$\varepsilon_{Hf}(t) = 10{,}000 \times ([(^{176}Hf/^{177}Hf)_S - (^{176}Lu/^{177}Hf)_S \times (e^{\lambda t} - 1)]/[(^{176}Hf/^{177}Hf)_{CHUR} - (^{176}Lu/^{177}Hf)_{CHUR} \times (e^{\lambda t} - 1)] - 1)$. S—Sample; t—measured zircon U-Pb ages in this study; CHUR—chondrite. $\lambda = 1.865 \times 10^{-11}$ a^{-1}. The $(^{176}Hf/^{177}Hf)_{CHUR}$ and $(^{176}Lu/^{177}Hf)_{CHUR}$ at present are 0.282772 and 0.0332, respectively.
#$T^{C}_{DM} = 1/\lambda \times \ln(1 + [(^{176}Hf/^{177}Hf)_S - (^{176}Hf/^{177}Hf)_{DM})]/[(^{176}Lu/^{177}Hf)_C - (^{176}Lu/^{177}Hf)_{DM}]) + t$. C—crust, DM—depleted mantle. The $(^{176}Hf/^{177}Hf)_{DM}$ and $(^{176}Lu/^{177}Hf)_{DM}$ at present are 0.283251 and 0.0384, respectively. $(^{176}Lu/^{177}Hf)_C = 0.015$.

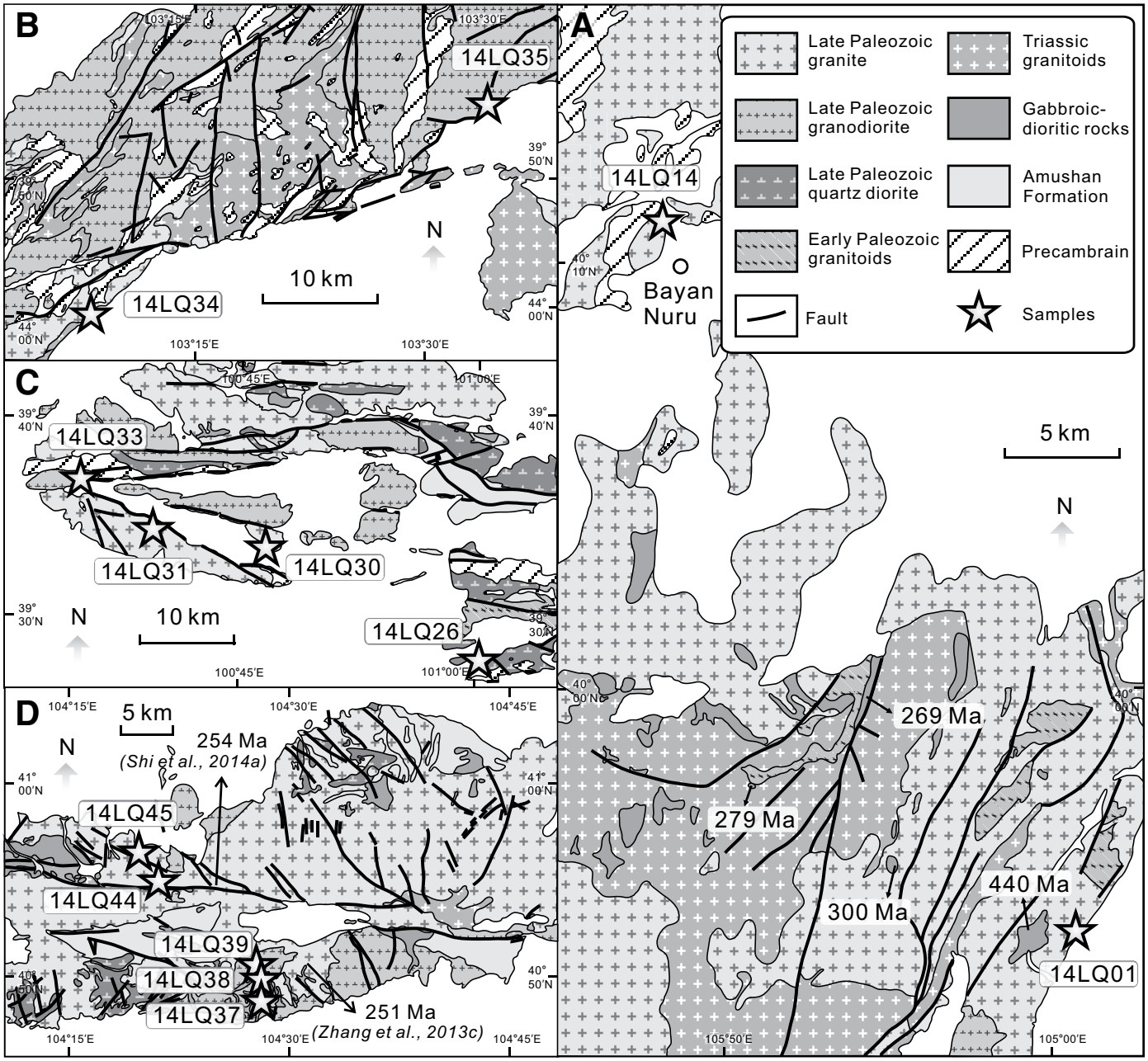

Figure 2. Geological maps of (A) the Bayan Nuru area (modified after 1:200,000 geological maps of the Alatanaobao, the Haobusi, the Qinggele, and the Jilantai areas); (B) the Yabulai area (after 1:200,000 geological maps of the Kunaitoulabamiao and the Aguimiao areas); (C) the Nuergai area (from 1:200,000 geological maps of the Pingchuan and the Nuergai areas); and (D) the Oliji area (from 1:200,000 geological map of the Oliji areas). Age data are cited from W. Zhang et al. (2013) and Shi et al. (2014a).

characterized by a varied rock assemblage of quartz diorite, granodiorite, and syenogranite (Fig. 2C). The relationship of these rock suites is unclear due to the paucity of outcrops and intense weathering.

Samples 14LQ26A–14LQ26C are weakly deformed quartz diorite with major mineral assemblages of hornblende (~20%), biotite (~10%–20%), plagioclase (50%–55%), and quartz (10%–20%) (Fig. 3D), of which hornblende is locally altered to epidote-zoisite. The syenogranite (samples 14LQ30A, 14LQ30B, and 14LQ31A) contains coarse-grained alkali feldspar of >50% (Fig. 3E) and biotite showing chlorite alteration, whereas the granodiorite (samples 14LQ33A and 14LQ33B) comprises more hornblende (10%–15%), biotite (~5%) and plagioclase (~40%). Plagioclase grains show local sericite alteration (Fig. 3F).

The Oliji Plutonic Complex

The Oliji plutonic complex in the middle part of the SLB intrudes the Amushan Formation and is crosscut by a Jurassic granitic porphyry (Fig. 2D). This plutonic complex is characterized by medium- to coarse-grained granodiorite (Fig. 3G) and monzogranite (Fig. 3H).

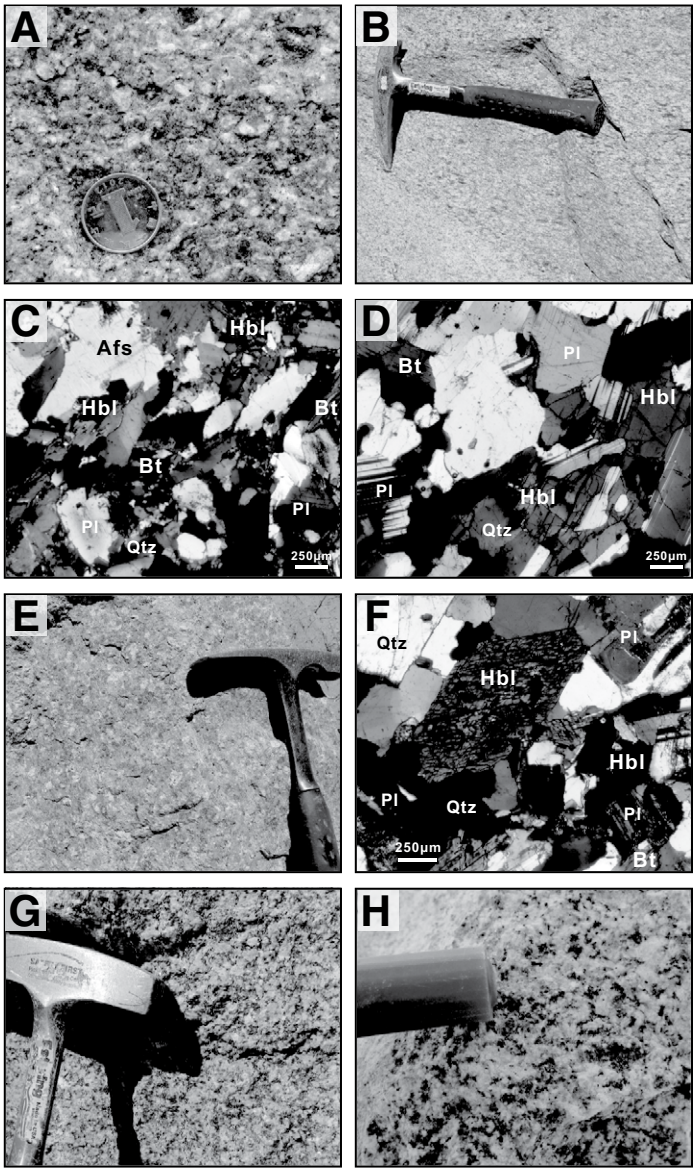

Figure 3. Representative field photographs and photomicrographs (crossed nicols): (A) Monzogranite showing a porphyritic texture in the Bayan Nuru plutonic complex; (B) granodiorite yielding weak gneissosity in the Yabulai plutonic complex; (C) sample 14LQ34A; (D) sample 14LQ26A; (E) coarse-grained syenogranite in the Nuergai plutonic complex; (F) sample 14LQ33A; (G) middle- to coarse-grained granodiorite in the Oliji plutonic complex; (H) middle- to coarse-grained monzogranite in the Oliji plutonic complex; Qtz—quartz; Afs—alkali feldspar; Pl—plagioclase; Hbl—hornblende; Bt—biotite.

The granodiorite (samples 14LQ37A and 14LQ37B, 14LQ38A and 14LQ38B, and 14LQ39A) is composed mainly of quartz (~30%), alkali feldspar (10%–20%), plagioclase (40%–50%), hornblende (3%–5%), and biotite (5%–10%), with minor epidote-zoisite, apatite, and sphene. Alkali feldspar and plagioclase grains show partially clay and sericite alteration, respectively. Hornblende and biotite grains occasionally show secondary alteration of chlorite and epidote-zoisite. Comparatively, four monzogranite samples (14LQ44A, 14LQ44B, 14LQ45A, and 14LQ45B) are characterized by more alkali feldspar (>30%) and quartz (35%–40%) with much less biotite. Occasional anhedral muscovite appears due to late alteration of biotite.

ANALYTICAL METHODS AND RESULTS

LA-ICPMS U-Pb Dating of Zircon

Prior to dating analysis for zircons, cathodoluminescence (CL) images were taken on a MonoCL3 attached to a scanning electron microscope (JSM-6510A, Japan) at Jinyu Technology Co., Ltd., Chongqing, China. Zircon U-Pb dating analysis was carried out using a laser ablation-inductively coupled plasma mass spectrometry (LA-ICPMS) at FocuMS Technology Co., Ltd., Nanjing, China. The system comprises a Photon Machines Excite 193nm laser ablation system and a quadrupole ICPMS (Agilent 7700x). The following were working parameters: 7 Hz repetition rate, 6.71 J/cm^2 energy, and 40 μm laser spot diameter. Zircon standard 91500 (Wiedenbeck et al., 1995) was used for U-Pb isotopic ratio correction, and zircon standard GJ-1 (Jackson et al., 2004) was used as unknown. A weighted mean $^{206}Pb/^{238}U$ age of 601 ± 5 Ma (n = 72) was obtained for the latter, in agreement with the recommended value of 600.4 ± 0.6 Ma (Jackson et al., 2004). Detailed zircon U-Pb isotopic data are listed in GSA Data Repository Table DR1[1].

Age of the Bayan Nuru Plutonic Complex

Zircons in a monzogranite sample 14LQ01A are euhedral and prismatic. They show oscillatory zoning in CL images (Fig. 4A) and high Th/U ratios of 0.50–0.87, indicating a magmatic origin. Fourteen analyses yield concentrated $^{206}Pb/^{238}U$ ages, with a weighted mean age of 268 ± 1 Ma (MSWD = 0.8; Fig. 4A), interpreted as the crystallization age of this monzogranite. One grain has an older age of 307 Ma, considered as a xenocrystic zircon in the monzogranite. Zircons from the syenogranite (sample 14LQ14A) are of a magmatic genesis, showing oscillatory zoning (Fig. 4B) and an average Th/U ratio of 0.48. Twenty-three analyses produce a weighted mean $^{206}Pb/^{238}U$ age of 281 ± 1 Ma (MSWD = 1.0; Fig. 4B). Taken together, the crystallization age of the Bayan Nuru granitic plutonic complex is 281–268 Ma.

Age of the Yabulai Plutonic Complex

Sample 14LQ34A is granodiorite, in which zircons are typical of a magmatic genesis with elongated prismatic forms, oscillatory zoning (Fig. 4C), and high Th/U ratios of >0.4. Nineteen analyses show similar $^{206}Pb/^{238}U$ ages between 280 Ma and 275 Ma, with a weighted mean age of 277 ± 1 Ma (MSWD = 0.8; Fig. 4C), interpreted as the crystallization age of this granodiorite. Similarly, 21 analyzed zircons from a monzogranite sample 14LQ35A also show oscillatory zoning (Fig. 4D) with high Th/U ratios and give a weighted mean $^{206}Pb/^{238}U$ age of 270 ± 1 Ma (MSWD = 1.2; Fig. 4D). Thus, the Yabulai plutonic complex yields a crystallization age of 277–270 Ma.

Age of the Nuergai Plutonic Complex

Zircons extracted from a quartz dioritic sample 14LQ26A have stubby prismatic forms (Fig. 4E). They show oscillatory zoning (Fig. 4E) and varying Th/U ratios from 0.50 to 1.17, reflecting a magmatic origin. Twenty-four analyzed grains have concentrated $^{206}Pb/^{238}U$ ages, with a weighted mean age of 269 ± 1 Ma (MSWD = 0.9; Fig. 4E), interpreted as the crystallization age of the quartz diorite. Samples 14LQ30A and 14LQ31A are monzogranite, in which zircons are commonly elongated in shape with ratio aspects of >3 (Figs. 4F and 4G) and characterized

[1]GSA Data Repository Item 2017237, Table DR1: Zircon U-Pb dating results; Table DR2: Zircon Hf-isotope compositions; and Table DR3: Whole-rock major- (wt%) and trace-element (ppm) compositions, is available at http://www.geosociety.org/datarepository/2017, or on request from editing@geosociety.org.

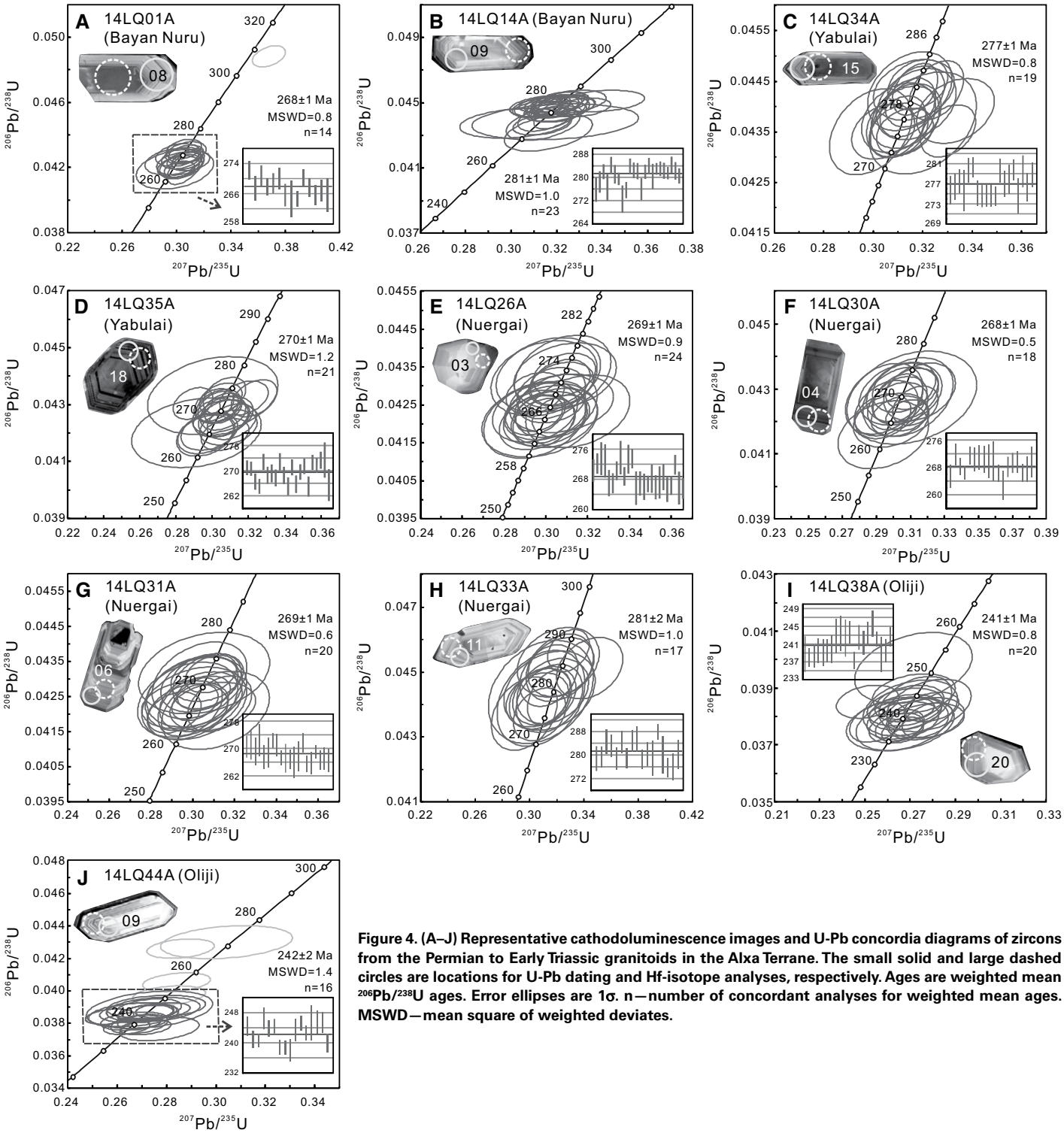

Figure 4. (A–J) Representative cathodoluminescence images and U-Pb concordia diagrams of zircons from the Permian to Early Triassic granitoids in the Alxa Terrane. The small solid and large dashed circles are locations for U-Pb dating and Hf-isotope analyses, respectively. Ages are weighted mean $^{206}Pb/^{238}U$ ages. Error ellipses are 1σ. n—number of concordant analyses for weighted mean ages. MSWD—mean square of weighted deviates.

by oscillatory zoning and high Th/U ratios of >0.4. Eighteen zircons in the former and 20 grains in the latter were analyzed and yield a similar weighted mean $^{206}Pb/^{238}U$ age of 268 ± 1 Ma (MSWD = 0.5; Fig. 4F) and 269 ± 1 Ma (MSWD = 0.6; Fig. 4G), respectively, indicating the crystallization age of the monzogranite. Zircons in another granodiorite sample 14LQ33A are of a magmatic origin with oscillatory zoning (Fig. 4H) and high Th/U ratios, 17 of which yield a weighted mean $^{206}Pb/^{238}U$ age of 281 ± 2 Ma (MSWD = 1.0; Fig. 4H), relatively older than that of the quartz diorite and monzogranite. Taken together, the crystallization age of the Nuergai plutonic complex is 281–268 Ma.

Age of the Oliji Plutonic Complex

Zircons from samples 14LQ38A and 14LQ44A show Th/U ratios varying from 0.39 to 1.10, and oscillatory zoning (Figs. 4I and 4J), indicative of a magmatic origin. Twenty analyses from the former and 16 from the latter yield an equal weighted mean $^{206}Pb/^{238}U$ age of 241 ± 1 Ma (MSWD = 0.8; Fig. 4I) and 242 ± 1 Ma (MSWD = 1.4; Fig. 4J), respectively, interpreted as the crystallization age of the Oliji granitoids. In addition, five inherited and/or xenocrystic zircons in sample 14LQ44A show older concordant $^{206}Pb/^{238}U$ ages between 271 Ma and 251 Ma, coincident with the giant Permian magmatic event (272–250 Ma) in the SLB (Ran et al., 2012; W. Zhang et al., 2013; Shi et al., 2014a, 2014b).

Zircon Hf-Isotope Compositions

Zircon Lu-Hf isotope analysis (presented in GSA Data Repository Table DR2) was conducted using a Neptune Plasma multi-collector ICPMS attached to a New Wave ArF 193 nm COMPex Pro laser ablation system at the State Key Laboratory of Mineral Deposits Research, Nanjing University (NJU), China. The adopted working parameters were: 44 μm ablation pit diameter, 8 Hz repetition rate, and 25 s ablation time. In order to monitor reliability and stability of the instrument, two reference zircon standards 91500 and Mud Tank were analyzed. Mean $^{176}Hf/^{177}Hf$ ratios of 0.282306 ± 0.000022 (n = 21) and 0.282502 ± 0.000017 (n = 22) were obtained, respectively, equal to suggested values for 91500 (0.282284 ± 0.000003; Wiedenbeck et al., 1995) and Mud Tank (0.282497 ± 0.000018; Hawkesworth and Kemp, 2006) within the error. In order to calculate the zircon initial $^{176}Hf/^{177}Hf$ ratios, $\varepsilon_{Hf}(t)$ values, depleted mantle model ages and two-stage model ages (T^C_{DM}), the following parameters were adopted. The decay constant is 1.865×10^{-11} per year for ^{176}Lu (Scherer et al., 2001). The $^{176}Hf/^{177}Hf$ and $^{176}Lu/^{177}Hf$ ratios for chondrite and depleted mantle at present are 0.282772 and 0.0332 (Blichert-Toft and Albarede, 1997) and 0.283251 and 0.0384 (Vervoort and Blichert-Toft, 1999), respectively. The $^{176}Lu/^{177}Hf$ ratio for the average continental crust is 0.015 (Griffin et al., 2002).

The ca. 268 Ma zircons from the Bayan Nuru plutonic complex show homogeneous and negative $\varepsilon_{Hf}(t)$ values from −6.1 to −3.2, and two-stage model ages (T^C_{DM}) of 1.67–1.49 Ga, whereas the ca. 281 Ma zircons in the Bayan Nuru plutonic complex yield relatively more negative $\varepsilon_{Hf}(t)$ values and older T^C_{DM} ages (Fig. 5A). The 277–270 Ma zircons from the Yabulai plutonic complex have more clustered and negative $\varepsilon_{Hf}(t)$ values (−7.4 to −3.0) and T^C_{DM} ages of 1.75–1.49 Ga (Fig. 5A). In contrast, different granitic samples from the Nuergai plutonic complex display positive $\varepsilon_{Hf}(t)$ values from +1.6 to +6.4 and corresponding younger T^C_{DM} ages of 1.20–0.89 Ga (Fig. 5A).

The ca. 241 Ma zircons in sample 14LQ38A from the Oliji plutonic complex display fairly positive $\varepsilon_{Hf}(t)$ values from +8.2 to +11.5 and young T^C_{DM} ages of 0.75–0.54 Ga, whereas those in sample 14LQ44A have more heterogeneous and enriched Hf-isotope compositions with $\varepsilon_{Hf}(t)$ values varying from −0.8 to +7.4, and older T^C_{DM} ages of 1.32–0.80 Ga (Fig. 5A). In addition, older zircons (256–271 Ma) in sample 14LQ44A show positive $\varepsilon_{Hf}(t)$ values of +5.0 to +7.7 (Fig. 5A).

Whole-Rock Major- and Trace-Element Compositions

Whole-rock major-element compositions were determined using an X-ray fluorescence (XRF) spectrometer at the NJU, and whole-rock trace-elemental analysis was carried out using a quadrupole ICPMS at the State Key Laboratory of Ore Deposit Geochemistry, Guiyang Institute of Geochemistry (GYIG), Chinese Academy of Sciences, China. Generally, analytical precisions for major- and trace-elements are higher than 2% and 5%, respectively. Analytical results are given in GSA Data Repository Table DR3.

Whole-Rock Major-Element Compositions

The Permian granitoids in the NLB display a large variation in major-element compositions with SiO_2 contents varying from 55.0% to 76.8% (Fig. 6). The 281–268 Ma Bayan Nuru granitoids and the 277–270 Ma Yabulai granodiorites show calc-alkaline to high-K calc-alkaline affinities (Fig. 6). They plot into the field of weakly peraluminous to metaluminous (Fig. 7A) and magnesian series (Fig. 7B), with molar $Al_2O_3/(CaO+Na_2O+K_2O)$ (A/CNK) values of 0.97–1.02 and low $FeO^t/(MgO + FeO^t)$ ratios of 0.47–0.82, more akin to I-type granitoids (Whalen et al., 1987). Comparatively, the 281–268 Ma Nuergai granitoids show a much

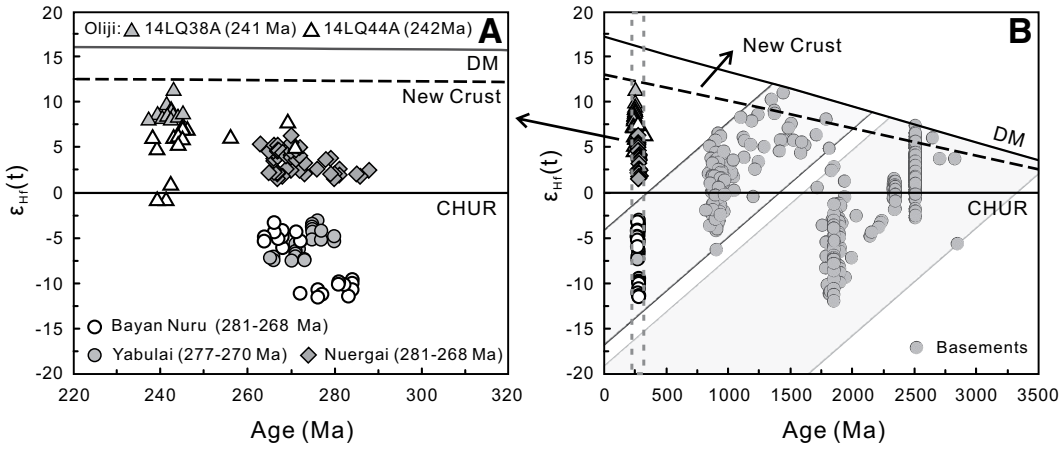

Figure 5. (A) and (B) Hf-isotope compositions of zircons from the Permian to Early Triassic granitoids in the Alxa Terrane. DM—depleted mantle; CHUR—chondrite. Data for the Precambrian basement rocks in the Alxa Terrane are from Geng and Zhou (2011), Dan et al. (2012, 2014b), Gong et al. (2012), and J.X. Zhang et al. (2013).

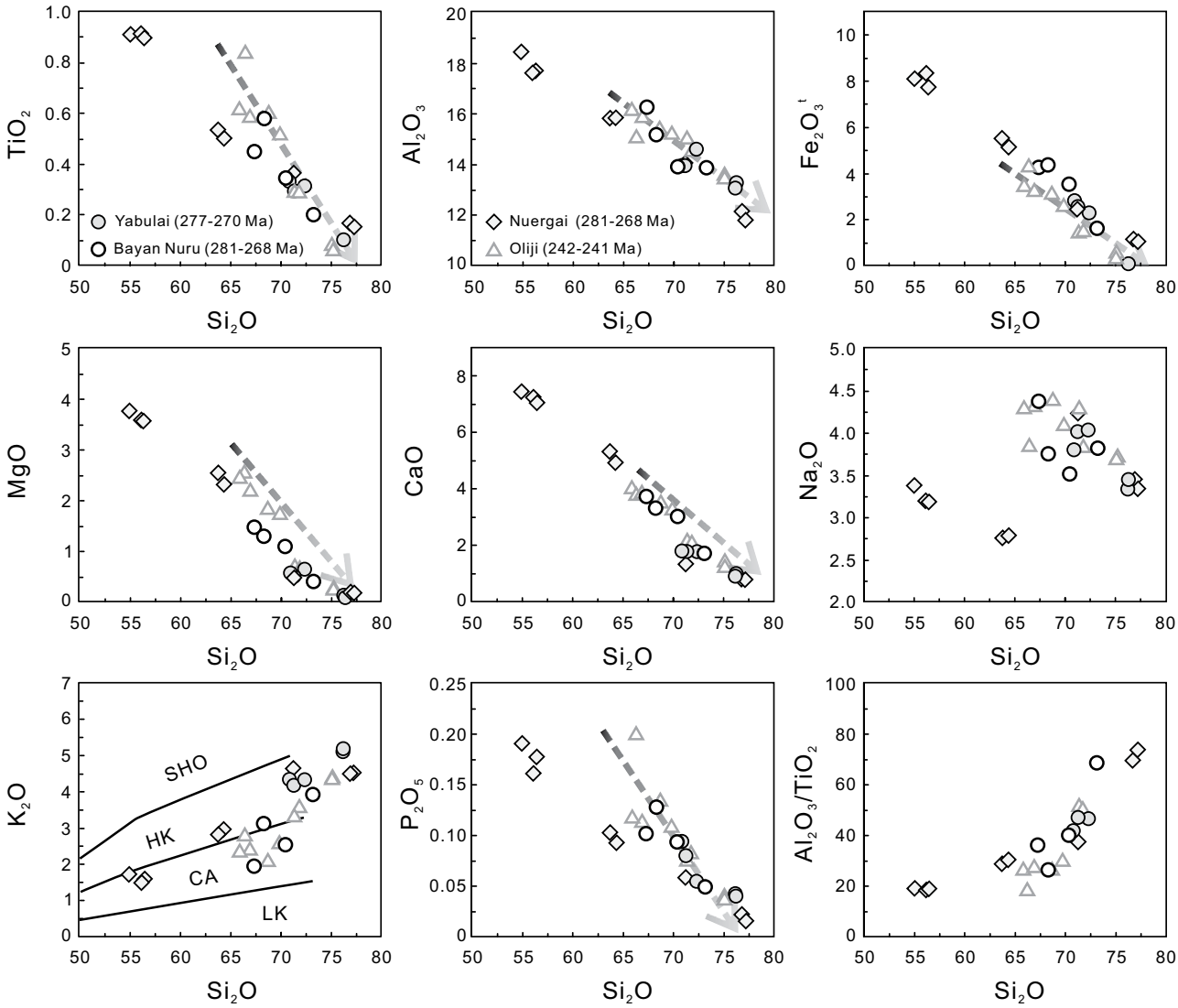

Figure 6. Harker diagrams of whole-rock major-element compositions. Solid lines in K_2O versus SiO_2 diagram are from Peccerillo and Taylor (1976). LK—low-K tholeiite series; CA—calc-alkaline series; HK—high-K calc-alkaline series; SHO—shoshonite series.

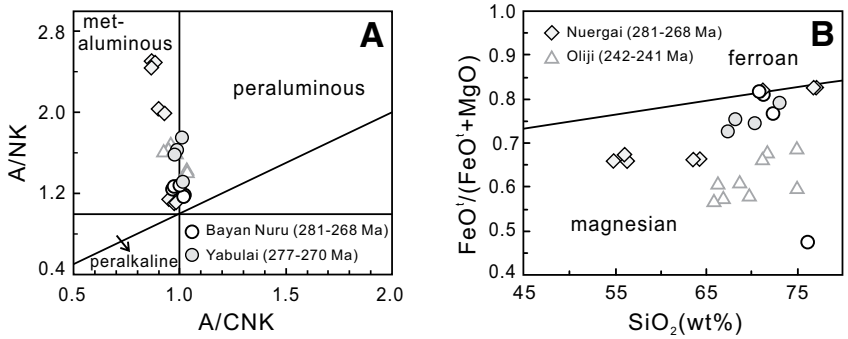

Figure 7. (A) Molar $Al_2O_3/(CaO + Na_2O + K_2O)$ (A/CNK) versus molar $Al_2O_3/(Na_2O + K_2O)$ (A/NK) diagram (Maniar and Piccoli, 1989); (B) $FeO^t/(FeO^t + MgO)$ versus SiO_2 diagram (after Frost et al., 2001).

larger variation in major-element compositions. They exhibit roughly lower Al_2O_3, Na_2O, K_2O, and P_2O_5 contents (Fig. 6) and lower A/CNK values (0.87–0.98) and Al_2O_3/TiO_2 ratios at similar silica contents than those of the Bayan Nuru and Yabulai counterparts, indicative of typical I-type affinities (Whalen et al., 1987).

In comparison, the ca. 241 Ma Oliji granitoids in the SLB have lower $Fe_2O_3^t$ and K_2O contents with lower $FeO^t/(MgO + FeO^t)$ and Al_2O_3/TiO_2 ratios at the same SiO_2 levels than those of the Permian granitoids from the NLB (Figs. 6 and 7). These Early Triassic granitoids show I-type features (Whalen et al., 1987), belonging to calc-alkaline to high-K calc-alkaline (Fig. 6), weakly peraluminous to metaluminous with A/CNK values of 0.92–1.04 (Fig. 7A), and magnesian series (Fig. 7B).

Whole-Rock Trace-Element Compositions

The Permian granitoids in the NLB and the Early Triassic granitoids in the SLB also show a broad range of trace-element compositions, with the former containing relatively lower transition elements (e.g., Sc, V, Cr, Co, and Ni) and Sr contents, higher Rb, Y, rare-earth elements (REEs) and Nb components, and higher Rb/Sr ratios.

Distinct REEs patterns are illustrated in Figures 8A and 8B. The Permian granitoids in the NLB exhibit varying REEs contents ranging from 81 ppm to 249 ppm, weak to medium REEs fractionation with light REEs (LREEs)/heavy REEs (HREEs) ratios of 5.80–9.49 and $(La/Yb)_N$ ratios of 5.29–10.30, and strongly to weakly negative Eu anomalies (Eu/Eu* = 0.11–0.87) (Fig. 8A). In contrast, except two monzogranite samples with fairly high silica contents, the Early Triassic granitoids in the SLB mostly display lower REEs contents of 46–135 ppm, stronger REEs fractionation with higher LREEs/HREEs and $(La/Yb)_N$ ratios, and less negative Eu anomalies (Eu/Eu* = 0.80–0.98) (Fig. 8B).

In the mid-ocean ridge basalt (MORB)–normalized, incompatible–trace-element spidergrams (Figs. 8C and 8D), almost all the Permian and Early Triassic granitoids in this study demonstrate relative depletions in high field strength elements (HFSEs, e.g., Nb, Ta, and Ti) and P and relative enrichments in K, Rb, and Ce.

DISCUSSION

Permian to Triassic Magmatic Episodes in the Alxa Terrane

LA–ICPMS zircon U-Pb dating on ten samples from four granitic plutonic complexes indicates a Permian to Triassic magmatic event in the Alxa Terrane. New results reveal that the crystallization age of the Bayan Nuru and Nuergai plutonic complexes is 281–268 Ma, roughly overlapping the age of the Yabulai plutonic complex at 277–270 Ma. Therefore, an episode of magmatism between 280 and 268 Ma took place in the Alxa Terrane, characterized by varied granitoids including quartz diorite, granodiorite, monzogranite, and syenogranite. This is consistent with previous studies that suggested a Permian magmatic event in the Alxa Terrane (e.g., Dan et al., 2014a, 2015b; Liu et al., 2016). Apart from the predominant granitoids, some 280–264 Ma ultramafic to intermediate magmatic rocks were also unveiled in the eastern part of the NLB and the middle part of the SLB (Feng et al., 2013; L. Zhang et al., 2013; Shi et al., 2014a; Liu et al., 2017).

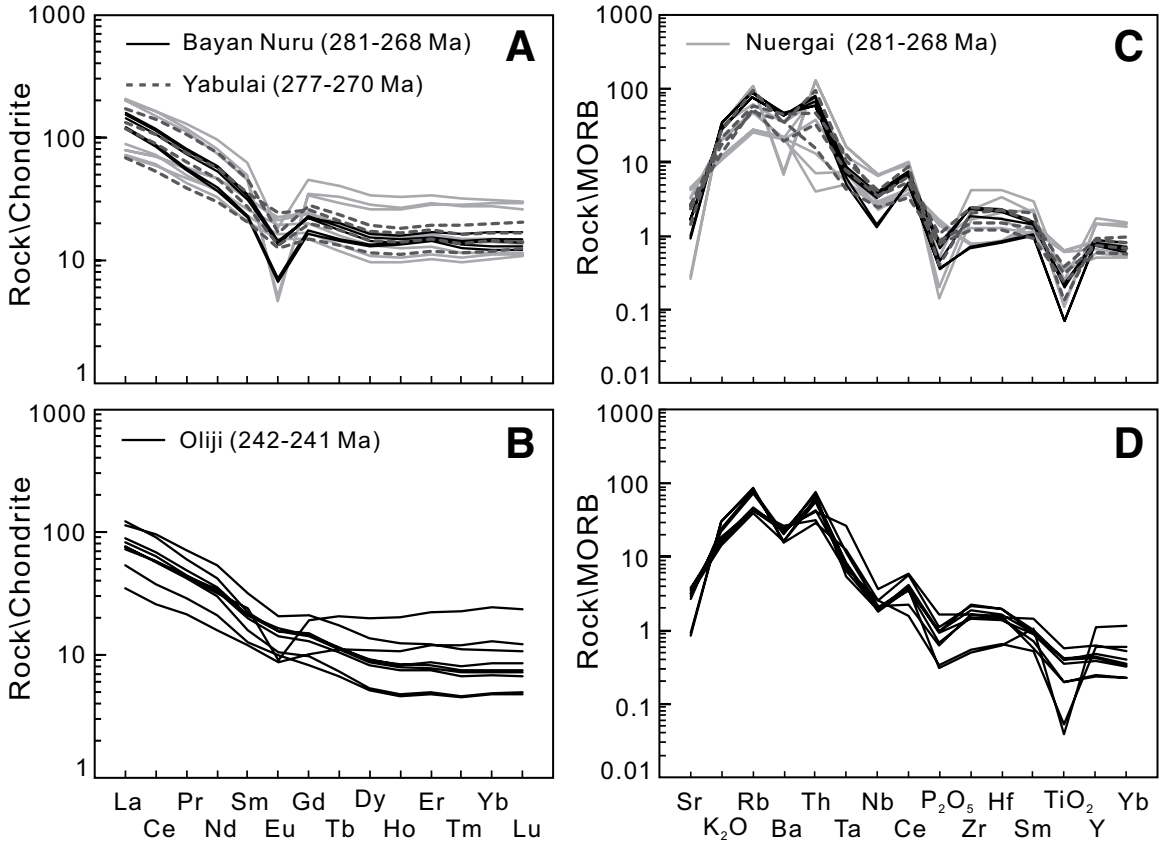

Figure 8. (A and B) Chondrite-normalized rare-earth element patterns; (C and D) mid-ocean ridge basalt (MORB)–normalized, incompatible-element abundances. Chondrite values are from McDonough and Sun (1995), and MORB values are from Pearce (1983).

This study also unveils that the Oliji granitoids were emplaced at ca. 241 Ma, slightly younger than the previous reported zircon U-Pb ages of 254–250 Ma for the nearby monzogranite and granodiorite from the Oliji plutonic complex (Fig. 2D) (W. Zhang et al., 2013; Shi et al., 2014a). Thus, the Oliji granitic plutonic complex most likely evolved in a period from the Latest Permian to the Early Triassic. In addition, coeval 255–239 Ma ultramafic to felsic plutonic rocks have also been identified in the SLB and the eastern part of the NLB (Zhang et al., 2010; Ran et al., 2012; Shi et al., 2014a, 2014b; Wang et al., 2015b).

Petrogenesis

Fractional Crystallization

The Bayan Nuru and Nuergai granitoids in this study contain a large variety of rock assemblages with crystallization ages ranging from 281 Ma to 268 Ma. Fractional crystallization can be the potential cause for such a large age span of different granitoids. If this is the case, the younger granitoids should have more felsic compositions. However, the ca. 268 Ma Bayan Nuru monzogranites yield lower SiO_2 contents than those of the ca. 281 Ma syenogranites, while the younger Nuergai quartz diorites show much less felsic compositions (Table DR3 [see footnote 1]). Such a long period of ca. 13 Ma is also unreasonable for a single fractional crystallization process. Therefore, fractional crystallization alone cannot explain the distinct geochemical compositions for the Bayan Nuru and Nuergai plutonic complexes.

The Yabulai and Oliji granitic plutonic complexes exhibit obvious linear correlations for major elements on the Harker diagrams (Fig. 6), suggesting a significant role of fractional crystallization. Negative correlations of TiO_2, Al_2O_3, $Fe_2O_3^t$, MgO, CaO, and P_2O_5 with respect to SiO_2 (Fig. 6) indicate fractional crystallization of mafic minerals (e.g., biotite and/or hornblende) and plagioclase with minor apatite and ilmenite. The positive correlation between K_2O and SiO_2 (Fig. 6) rules out the possibility of fractionation of alkali feldspar or biotite. Accordingly, the Yabulai and Oliji granitoids show fractional crystallization of hornblende + plagioclase + ilmenite + apatite. However, fractional crystallization alone cannot explain the distinct geochemical compositions of these granitoids, especially in terms of their distinct REE patterns and zircon Hf-isotope compositions.

To conclude, heterogeneous sources were probably a more important factor in controlling the petrogenesis of the Permian and Early Triassic granitoids in this study.

Sources

The 281–268 Ma Bayan Nuru granitoids and the 277–270 Ma Yabulai granitoids show homogenous and enriched zircon Hf-isotope compositions with negative $\varepsilon_{Hf}(t)$ values and old T^C_{DM} ages of 2.01–1.49 Ga, suggesting the involvement of the Precambrian basement rocks as source materials. The Neoarchean to Paleoproterozoic basements in the Alxa Terrane are excluded because they have fairly older T^C_{DM} ages of >2.5 Ga (Fig. 5B). The Neoproterozoic rocks in the region can potentially be source materials, since the zircon Hf-isotope evolutionary array of these rocks covers the zircon $\varepsilon_{Hf}(t)$ values of the Bayan Nuru and Yabulai granitic plutonic complexes, despite different rock types (Fig. 5B). These Neoproterozoic rocks are sporadically exposed in the eastern and southwestern parts of the NLB and consist mainly of predominant 970–840 Ma gneissic granitoids and metasedimentary sequences yielding youngest detrital zircon ages of 910–810 Ma and minor 830–800 Ma ultramafic intrusions and felsic volcanic rocks (Geng et al., 2002; Li et al., 2004; Geng and Zhou, 2010; Peng et al., 2010; Dan et al., 2014b; Hu et al., 2014; Tang et al., 2014). Among these rock units, the Neoproterozoic granitoids and felsic volcanic rocks show high silica contents of mostly >70% (Peng et al., 2010; Geng and Zhou, 2011; Dan et al., 2014b), unlikely to generate the various granitoids from the Bayan Nuru and Yabulai plutonic complexes. In addition, the metasedimentary rocks cannot produce these I-type granitic magmas, and the ultramafic intrusions are also excluded because it is difficult for granites to be generated by progressive fractional crystallization of mafic magmas (e.g., Clemens et al., 2011; Clemens and Stevens, 2012; Nandedkar et al., 2014). Alternatively, we suggest that the mixing of quartzofeldspathic rocks (i.e., granitoids and/or metasedimentary rocks) and ultramafic rocks might have been the potential candidates for source materials of these I-type granitoids, as evidenced by a large amount of geochemical modeling works (e.g., Gray, 1984; Patiño Douce, 1995, 1999; Collins, 1998; Moyen et al., 2001). The various inputs of mixing members can contribute to the distinct geochemical compositions for the Bayan Nuru plutonic complex.

In comparison, the 281–268 Ma granitoids from the Nuergai plutonic complex in the western part of the NLB show more concentrated and radiogenic zircon Hf-isotope compositions with positive $\varepsilon_{Hf}(t)$ values and relatively younger T^C_{DM} ages of 1.20–0.89 Ga. However, no pre-Permian rocks in the Alxa Terrane have the same Meso- to Neoproterozoic model ages to generate these granitoids. Instead, the Hf-isotope continuum of the Nuergai granitoids lies between a mantle-like component and the package of the Neoproterozoic rocks in the region, possibly due to crust-mantle magma mixing during their genesis. This interpretation is in accordance with I-type affinities of the Nuergai granitoids because such rocks are commonly considered to form in magma mixing processes (e.g., Gray, 1984; Foden et al., 2002; Griffin et al., 2002; Yu et al., 2005; Kemp et al., 2007, 2009). In order to quantify the proportions of crust- and mantle-derived materials, a simplified dual-members mixing model is adopted (Liu and Chen, 1991). In this model, the Neoproterozoic component in the region is assumed to be the evolved end member. This crust-derived magma is assumed to have zircon Hf-isotope compositions of these Neoproterozoic rocks (Geng and Zhou, 2011; Dan et al., 2014b), while an average Hf content of this crust-derived magma is equal to that of the Bayan Nuru and Yabulai granitoids that were sourced from these basement rocks. We adopt a Hf-isotope component of "New Crust" proposed by Dhuime et al. (2011) as that of the juvenile end member, and an average Hf content of this juvenile magma is equal to that of average arc basalts and andesites (Kelemen et al., 2003). Our calculated results show that ~70% mantle-derived materials should have been added to generate the Nuergai granitoids. If the crust member involves older Archean to Paleoproterozoic basements in the region, the proportion of the juvenile materials would be larger. The geochemical heterogeneity of the Nuergai granitoids can be explained by various proportions of crust- and mantle-derived materials.

Similarly, the ca. 242 Ma monzogranite from the Oliji plutonic complex in the SLB displays a large variation of zircon $\varepsilon_{Hf}(t)$ values ranging from −0.8 to +7.4, also consistent with the crust-mantle magma mixing model. In contrast, the ca. 241 Ma granodiorite in the Oliji plutonic complex shows fairly positive zircon $\varepsilon_{Hf}(t)$ values from +8.2 to +11.5, reflecting primarily mantle-derived materials. Calculated results of the simplified dual members mixing model suggest that ~76% mafic end member may have been added in producing the monzogranite magma and up to 90% for the granodiorite with such depleted zircon Hf-isotope compositions. Such a large proportion emphasizes a considerably significant role of juvenile materials that are most likely the newly accreted lower crust.

Tectonic Setting

Permian Granitoids

A giant Permian granitic flare-up has been identified in the Alxa Terrane, whose tectonic setting, however, is still controversial, with different

models advocating oceanic subduction, post-collisional, or mantle-plume settings (Ran et al., 2012; Shi et al., 2012; L. Zhang et al., 2013; W. Zhang et al., 2013; Dan et al., 2014a; Lin et al., 2014; Hu et al., 2015; Wang et al., 2015b).

The mantle-plume setting seems inadequate to account for the relatively smaller size (~0.05 Mkm^2) of the Permian granitic event in the Alxa Terrane than that of common silicic igneous provinces (>0.10 Mkm^2; Bryan, 2007). Furthermore, mantle-plume–associated high-temperature continental flood basalts and komatiitic sequences (e.g., Campbell et al., 1989; Campbell and Griffiths, 1990) are lacking in the Alxa Terrane.

The post-collisional setting is also not preferred. The Permian magmatism was widespread both along the northern margin of the NCC and on the Alxa Terrane (Liu et al., 2016). Such a ~2000-km-long linear magmatic belt cannot be interpreted in a post-collisional setting. In addition, the Early Permian porphyries in the eastern part of the Alxa Terrane experienced north-vergent deformation (Lin et al., 2014), which is amenable to a compressional south-dipping subduction setting, rather than an extensional post-collisional setting.

We thus favor the subduction setting in interpreting the origin of the Permian magmatic rocks in the Alxa Terrane based on the following lines of evidence:

(1) This study has revealed that the 281–268 Ma Nuergai granitoids were sourced from mixing magmas from the Neoproterozoic basements and mantle-derived materials, which is prone to occur in a subduction setting (e.g., Gill, 1981; Blundy and Sparks, 1992; Tepley et al., 2000; Zhou and Li, 2000; Annen et al., 2006; Reubi and Blundy, 2009).

(2) The zircon-saturation temperature calculated from whole-rock compositions of granitoids has been a powerful tool to estimate the crystallization temperature of magma at the time when zircon forms (Watson and Harrison, 1983). The calculated results reveal that most of the Permian granitic samples have low crystallization temperatures of 803–670 °C (Table DR3 [see footnote 1]). These low-temperature, I-type granitoids are more inclined to form at the high flux of water in a subduction setting (e.g., Hermann and Green, 2001; Collins et al., 2016), which goes against the mantle-plume or post-collisional models.

(3) A database has been compiled concerning the available zircon $\varepsilon_{Hf}(t)$ and whole-rock $\varepsilon_{Nd}(t)$ values in the Late Carboniferous to Triassic magmatic rocks in the Alxa Terrane. The increasingly evolved isotope compositions during Late Carboniferous to Middle Permian time (Figs. 9A and 9B) are in agreement with an advancing compressional subduction setting, instead of an extensional setting in the post-collisional or mantle-plume regimes (e.g., Kemp et al., 2009; Collins et al., 2011; Roberts et al., 2013; Han et al., 2016a).

(4) Coeval 280–268 Ma ultramafic to intermediate intrusions showing arc-like geochemical affinities have also been reported in the eastern part of the NLB, in favor of a subduction regime (Feng et al., 2013; L. Zhang et al., 2013; Liu et al., 2017).

Early Triassic Granitoids

The Early Triassic Oliji granitoids in this study are considered to form in a post-collisional setting according to following reasons:

(1) These Early Triassic granitic magmas show juvenile isotopic compositions (Fig. 5A), placing a predominant role of mantle-derived materials in magma generation. This is amenable to occurring in an extensional setting where asthenospheric mantle is prone to ascend and partially melt (e.g., Liégeois et al., 1998; Sylvester, 1998; Chen and Arakawa, 2005; Yang et al., 2008).

(2) The compiled zircon $\varepsilon_{Hf}(t)$ and whole-rock $\varepsilon_{Nd}(t)$ values of the magmatic rocks in the Alxa Terrane show an increasingly depleted trend from the Middle Permian to the Triassic (Figs. 9A and 9B), which may be attributed to the involvement of mantle-derived magmas in an extensional setting (e.g., Kemp et al., 2009; Collins et al., 2011).

(3) The 256–249 Ma high-K calc-alkaline granitoids and 266–250 Ma bimodal intrusive associations with radiogenic isotopic compositions have also been identified in the Alxa Terrane, indicating an extensional setting in a post-collisional regime since the Late Permian (W. Zhang et al., 2013; Lin et al., 2014; Shi et al., 2014a, 2014b).

Constraints on the Timing of the Final Closure of the PAO

The identification of the closure of a major ocean can be sufficiently clued from convergent high-strain zones with large-scale thrust faults and regional high-grade metamorphism, blueschist mélanges, and ophiolite remnants (e.g., Dewey and Şengör, 1979). However, unlike Himalaya-type collision, the middle and eastern segments of the PAO closed as a result of multiple accretionary processes via double-sided subduction, lacking the records of intensive deformation and high-grade metamorphism (e.g., Xiao et al., 2003; Eizenhöfer et al., 2014). In addition, the reservation of blueschist and ophiolite remnants in the Alxa Terrane is also scarce. The ca. 300 Ma Enger Us and ca. 275 Ma Quagan Qulu ophiolitic mélanges sporadically outcrop along two faults in the region, considered as a late Paleozoic ocean-arc system (Zheng et al., 2014), which only implies that the PAO did not completely disappear prior to Early Permian.

Nevertheless, the radiometric isotopic signatures of igneous rocks primarily reflect the characteristics of magma sources; samples show a large spread of zircon $\varepsilon_{Hf}(t)$ values probably attributed to magma mixing processes, whereas samples exhibit concentrated zircon $\varepsilon_{Hf}(t)$ values reflecting single old crustal or juvenile source domain. Numerous recent studies have efficiently correlated the variation of radiometric isotope signatures, especially zircon $\varepsilon_{Hf}(t)$ and whole-rock $\varepsilon_{Nd}(t)$ values, with large-scale switching tectonics (e.g., Jahn et al., 2000; Griffin et al., 2002; Kemp et al., 2009; Collins et al., 2011; Roberts et al., 2013; Smits et al., 2014; Boekhout et al., 2015; Han et al., 2016a; Liu et al., 2016). A major tectonic change (e.g., advancing-retreating subduction transition, oceanic closure, or collision) inevitably affects the magma sources and petrogenetic processes of igneous rocks, and hence changes their isotopic characteristics.

In general, a compressional geodynamic setting sees isotopic excursion to more enriched compositions (e.g., Smits et al., 2014; Boekhout et al., 2015; Han et al., 2016a; Liu et al., 2016), which is the case in the Alxa Terrane during Late Carboniferous to Middle Permian time (Figs. 9A and 9B). In this scenario, the advancing subduction of the PAO produced compression in the overriding Alxa Terrane and resulted in a local increase in crustal thickness and a larger degree of subduction erosion, leading to greater crustal assimilation and more enrichment of the mantle. Accordingly, gradually evolved isotope signatures were recorded in the magmatic arc (Figs. 9A and 9B). In contrast, an extensional setting exhibits excursion to more juvenile isotopes (e.g., Smits et al., 2014; Han et al., 2016a), which is also the case in this study; the Middle Permian to Triassic magmatic rocks in the Alxa Terrane demonstrate increasing $\varepsilon_{Hf}(t)$ and $\varepsilon_{Nd}(t)$ values (Figs. 9A and 9B), and the majority of the Triassic zircons exhibit fairly positive $\varepsilon_{Hf}(t)$ values (>+5; Fig. 9A), suggesting primarily juvenile materials as magma source. This extensional setting most likely corresponds to the closure of oceanic domains with collision or accretion events (e.g., Smits et al., 2014) or a retreating arc in the oceanic subduction regime (e.g., Han et al., 2016a). The former model is preferred on the basis of the 256–249 Ma high-K calc-alkaline granitoids and 266–250 Ma bimodal intrusive associations recognized in the region that have been considered to form in a post-collisional regime (W. Zhang et al., 2013; Lin et al., 2014; Shi et al., 2014a, 2014b). In this case, following the closure

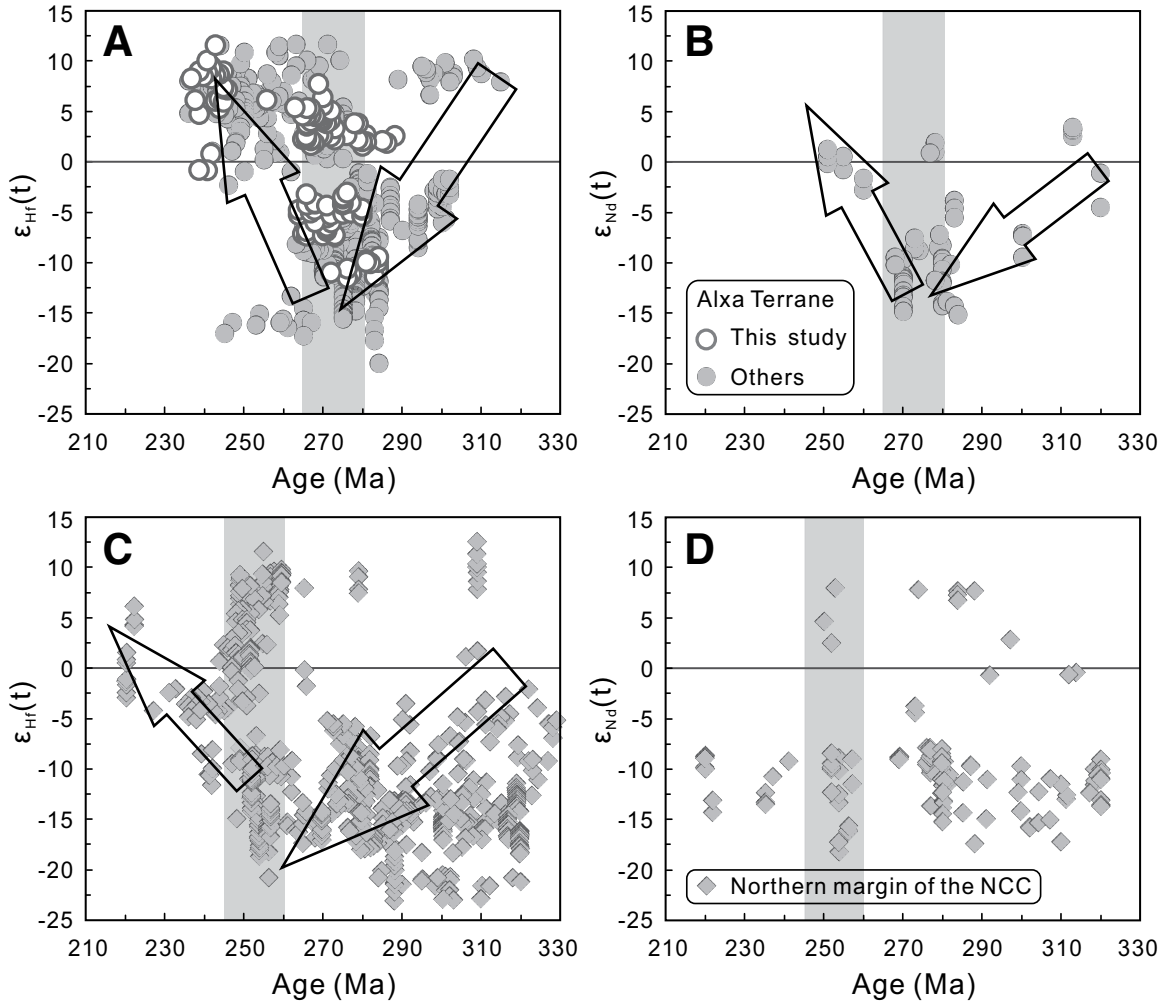

Figure 9. (A and B) Zircon $\varepsilon_{Hf}(t)$ and (C and D) whole-rock $\varepsilon_{Nd}(t)$ values versus ages from the Late Carboniferous to Triassic magmatic rocks in the Alxa Terrane and the northern margin of the North China Craton (NCC). Data for other Late Carboniferous to Triassic magmatic rocks in the Alxa Terrane are from Pi et al. (2010), Peng et al. (2013), Wu et al. (2013), W. Zhang et al. (2013), Dan et al. (2014a, 2015b), Shi et al. (2014a, 2014b), and Hu et al. (2015). Data for other counterparts on the northern margin of the NCC are from Luo et al. (2004, 2007, 2013), Zhang et al. (2004, 2009a, 2009b, 2009c, 2010, 2011, 2012a, 2012b), Jiang et al. (2007), Tian et al. (2007), Chen et al. (2009), Feng et al. (2009), Wang et al. (2009), Jian et al. (2010), Hou et al. (2011), Zhao et al. (2011), Cao et al. (2013), Mo et al. (2014), and Wang et al. (2015a, 2015b).

of the PAO lithosphere, the overriding Alxa Terrane probably underwent crustal thinning in a post-collisional setting. In this scenario, the asthenospheric mantle was upwelled, partially melted, and underplated, finally resulting in magmas with more juvenile isotope signatures. Notably, in the transitional period of ca. 280–265 Ma, a marked shift with a very large spread of positive to negative $\varepsilon_{Hf}(t)$ and $\varepsilon_{Nd}(t)$ values illustrating a mixed magma source can be identified, corresponding to a tectonic switch from subduction to post-collision due to the closure of the PAO. In this scenario, various crustal and mantle components could be involved during magma generation, such as old crustal materials, enriched lithospheric mantle, and depleted asthenospheric mantle. The involvement of different proportions of crust- and mantle-derived materials possibly produced magmas having heterogeneous isotope compositions with a very large spread of positive to negative zircon $\varepsilon_{Hf}(t)$ and whole-rock $\varepsilon_{Nd}(t)$ values (e.g., Smits et al., 2014). Similar cases in which a marked shift with a large variation of isotopes is related to the final closure of a major ocean also occurred in the adjacent areas and worldwide, including ca. 310–300 Ma closure of the western segment of the PAO along the northern margin of the Tarim Craton (Han et al., 2016b; Zhang et al., 2016a) and ca. 1.2–1.1 Ga assembly of the Proterozoic Australia among the North, West, and South Australian cratons (Smits et al., 2014). In addition, a Hf-isotope gap is also documented in the Alxa Terrane during the transitional period, which might have recorded the heterogeneity of the magma source in different locations (Figs. 9A and 9B).

The transitional period of 280–265 Ma is also in accordance with the sedimentary records in the Alxa Terrane. Xie et al. (2014) identified the late Middle Permian to the early Late Permian deep-water radiolarians fossils, i.e., albaillellarians, in the exotic siliceous rocks from the ca. 300 Ma Enger Us ophiolitic mélange, supporting that the final disappearance of the middle segment of the PAO should have occurred after the Late Permian. Moreover, the sedimentological history of the Late Carboniferous to Early Permian Amushan Formation suggests that the PAO might

have begun to close in the Early Permian (Lu et al., 2012; W. Zhang et al., 2013). The lower and middle sequences of this formation contain 320–302 Ma mafic to felsic volcanic rocks, clastic rocks, and carbonates, representing oceanic arc and back-arc basin environments. In contrast, the upper sequence of the formation changes to molasse deposition, including silty shale, sandstone, gravel-bearing sandstone, and conglomerate, which indicates the swallowing basin from the Late Carboniferous to Early Permian.

Furthermore, a structural analysis in the Langshan area in the eastern part of the Alxa Terrane (Lin et al., 2014) reveals north-vergent deformation for Early Permian porphyries (290–280 Ma) and non-deformation for Late Permian dolerites (256 Ma). This implies a tectonic change from south-dipping subduction to post-collision between 280 Ma and 256 Ma, supporting our interpretation that the final closure of the PAO most likely occurred at 280–265 Ma.

Eastward Closing of the PAO during Late Carboniferous to Middle Triassic Time

Available data show that a ~2000-km-long, ENE-stretching Paleozoic magmatic belt developed on the northern margin of the NCC; this belt is considered to extend westerly to the Alxa Terrane (summarized in Liu et al., 2016). For comparison, the zircon $\varepsilon_{Hf}(t)$ values of Late Carboniferous to Triassic magmatic rocks on the northern margin of the NCC are illustrated in Figure 9C. It is noteworthy that 330–250 Ma zircons display a large spread and roughly decreasing $\varepsilon_{Hf}(t)$ values with time (Fig. 9C). Most importantly, a marked shift with a large variation of positive to negative $\varepsilon_{Hf}(t)$ values appears at 260–245 Ma (Fig. 9C), which is seemingly also present on the whole-rock $\varepsilon_{Nd}(t)$ values versus age diagram (Fig. 9D). Subsequently, the isotopic values in the Triassic exhibit an overall increasing trend (Figs. 9C and 9D). Accordingly, a complexity of a mixing source in the Late Permian to Early Triassic and an increasingly juvenile source during Triassic time can be inferred. Such a marked change of Hf and Nd isotopic arrays and a subsequent increasing trend are similar but posterior to those in the Alxa Terrane and most likely reflect the timing of the main tectonic switch from subduction to post-collision orogenesis on the northern margin of the NCC. Moreover, a majority of previous paleogeographic, geochronologic, geochemical, and structural investigations also support that the final closure of the PAO on the northern margin of the NCC occurred in the Late Permian to Middle Triassic (Xiao et al., 2003, 2015; Zhang et al., 2004, 2007, 2009a, 2009b, 2009c, 2012b; Miao et al., 2007; Windley et al., 2007; Jian et al., 2008; Chen et al., 2009; Wilhem et al., 2012; Cao et al., 2013; Eizenhöfer et al., 2014, 2015a, 2015b; Wang et al., 2015a). Therefore, we conclude that the closure time of the PAO on the northern margin of the NCC, probably between 260 and 245 Ma, is slightly younger than that in the Alxa Terrane at 280–265 Ma.

Previous studies have proposed that the PAO completely closed in the Late Carboniferous on the western margin of the Tarim Craton, and the Latest Carboniferous to Early Permian on its eastern margin (e.g., Gao et al., 2011; Han et al., 2011, 2016b; Klemd et al., 2011; Xiao et al., 2015; Zhang et al., 2015a, 2015b, 2016a, 2016b). Taken together, it can be inferred that a notably eastward closing process of the PAO took place during Late Carboniferous to Early Permian time along the northern margin of the Tarim Craton, at the latest Early Permian to Middle Permian in the Alxa Terrane, and in the Late Permian to Middle Triassic on the northern margin of the NCC.

CONCLUSIONS

(1) New LA-ICPMS zircon U-Pb dating results reveal that the emplacement of Bayan Nuru-Nuergai, Yabulai, and Oliji granitoids occurred at 281–268 Ma, 277–270 Ma, and ca. 241 Ma, respectively, suggesting a Permian to Triassic magmatic event in the Alxa Terrane.

(2) Whole-rock geochemical and zircon Hf-isotopic data suggest that the Permian Bayan Nuru and Yabulai granitoids were sourced primarily from the Neoproterozoic rocks in the Alxa Terrane, whereas the Permian Yabulai granitoids were derived from magma mixing of crust- and mantle-derived materials, and the Early Triassic Oliji granitoids involved more prominent mantle-derived materials.

(3) The marked shift of zircon $\varepsilon_{Hf}(t)$ and whole-rock $\varepsilon_{Nd}(t)$ values at 280–265 Ma demonstrates a robust tectonic switch from subduction to post-collision, corresponding to the timing of the final closure of the PAO in the Alxa Terrane.

(4) An eastward closure of the PAO is inferred, i.e., in the Late Carboniferous to Early Permian along the northern margin of the Tarim Craton, at 280–265 Ma in the Alxa Terrane, and at 260–245 Ma on the northern margin of the NCC.

ACKNOWLEDGMENTS

This study was financially supported by the National Natural Science Foundation of China (NSFC) Project (41190075) entitled, "Final Closure of the Paleo-Asian Ocean and Reconstruction of East Asian Blocks in Pangea," which is the fifth research project in the NSFC Major Program (41190070), "Reconstruction of East Asian Blocks in Pangea," Hong Kong Research Grants Council (RGC) General Research Fund (GRF) (grants HKU7063/13P and 17301915), NSFC General Projects (grants 41230207 and 41390441), and University of Hong Kong (HKU) Seed Funding Program for Basic Research (grant 201311159126). We are grateful to Gang Zeng, Jianfeng Gao, Liang Li, and Tao Yang for their kind assistance in sample preparation and experimental analyses.

REFERENCES CITED

Annen, C., Blundy, J.D., and Sparks, R.S.J., 2006, The genesis of intermediate and silicic magmas in deep crustal hot zones: Journal of Petrology, v. 47, p. 505–539, doi:10.1093/petrology/egi084.

BGMRIM (Bureau of Geology and Mineral Resources of Inner Mongolia Autonomous Region), 1991, Regional Geology of Inner Mongol Autonomous Region: Beijing, Geological Publishing House, 725 p. (in Chinese).

Blichert-Toft, J., and Albarede, F., 1997, The Lu-Hf isotope geochemistry of chondrites and the evolution of the mantle-crust system: Earth and Planetary Science Letters, v. 148, p. 243–258, doi:10.1016/S0012-821X(97)00040-X.

Blundy, J.D., and Sparks, R.S.J., 1992, Petrogenesis of mafic inclusions in granitoids of the Adamello Massif, Italy: Journal of Petrology, v. 33, p. 1039–1104, doi:10.1093/petrology/33.5.1039.

Boekhout, F., Roberts, N.M.W., Gerdes, A., and Schaltegger, U., 2015, A Hf-isotope perspective on continent formation in the south Peruvian Andes: Geological Society of London, Special Publications, v. 389, p. 305–321, doi:10.1144/SP389.6.

Bryan, S., 2007, Silicic large igneous provinces: Episodes, v. 30, p. 20–31.

Campbell, I.H., and Griffiths, R.W., 1990, Implications of mantle plume structure for the evolution of flood basalts: Earth and Planetary Science Letters, v. 99, p. 79–93, doi:10.1016/0012-821X(90)90072-6.

Campbell, I.H., Griffiths, R.W., and Hill, R.I., 1989, Melting in an Archaean mantle plume: Heads it's basalts, tails it's komatiites: Nature, v. 339, p. 697–699, doi:10.1038/339697a0.

Cao, H.H., Xu, W.L., Pei, F.P., Wang, Z.W., Wang, F., and Wang, Z.J., 2013, Zircon U-Pb geochronology and petrogenesis of the Late Paleozoic–Early Mesozoic intrusive rocks in the eastern segment of the northern margin of the North China Block: Lithos, v. 170, p. 191–207, doi:10.1016/j.lithos.2013.03.006.

Charvet, J., Shu, L.S., and Laurent-Charvet, S., 2007, Paleozoic structural and geodynamic evolution of eastern Tianshan (NW China): Welding of the Tarim and Junggar plates: Episodes, v. 30, p. 162–186.

Charvet, J., Shu, L.S., Laurent-Charvet, S., Wang, B., Faure, M., Cluzel, D., Chen, Y., and De Jong, K., 2011, Palaeozoic tectonic evolution of the Tianshan belt, NW China: Science China. Earth Sciences, v. 54, p. 166–184, doi:10.1007/s11430-010-4138-1.

Chen, B., and Arakawa, Y., 2005, Elemental and Nd-Sr isotopic geochemistry of granitoids from the West Junggar fold belt (NW China), with implications for Phanerozoic continental growth: Geochimica et Cosmochimica Acta, v. 69, no. 5, p. 1307–1320, doi:10.1016/j.gca.2004.09.019.

Chen, B., Suzuki, K., Tian, W., Jahn, B.M., and Ireland, T., 2009, Geochemistry and Os-Nd-Sr isotopes of the Gaositai Alaskan–type ultramafic complex from the northern North China craton: Implications for mantle-crust interaction: Contributions to Mineralogy and Petrology, v. 158, p. 683–702, doi:10.1007/s00410-009-0404-7.

Chen, N.H.C., Zhao, G.C., Jahn, B.M., Zhou, H., and Sun, M., 2017, Geochemistry and geochronology of the Delinggou Intrusion: Implications for the subduction of the Paleo-Asian Ocean beneath the North China Craton: Gondwana Research, v. 43, p. 178–192, doi:10.1016/j.gr.2016.01.007.

Clemens, J.D., and Stevens, G., 2012, What controls chemical variation in granitic magmas?: Lithos, v. 134, p. 317–329, doi:10.1016/j.lithos.2012.01.001.

Clemens, J.D., Stevens, G., and Farina, F., 2011, The enigmatic sources of I-type granites: The peritectic connexion: Lithos, v. 126, no. 3, p. 174–181, doi:10.1016/j.lithos.2011.07.004.

Collins, W.J., 1998, Evaluation of petrogenetic models for Lachlan Fold Belt granitoids: Implications for crustal architecture and tectonic models: Australian Journal of Earth Sciences, v. 45, p. 483–500, doi:10.1080/08120099808728406.

Collins, W.J., Belousova, E.A., Kemp, A.I.S., and Murphy, J.B., 2011, Two contrasting Phanerozoic orogenic systems revealed by hafnium isotope data: Nature Geoscience, v. 4, p. 333–337, doi:10.1038/ngeo1127.

Collins, W.J., Huang, H.Q., and Jiang, X., 2016, Water-fluxed crustal melting produces Cordilleran batholiths: Geology, v. 44, no. 2, p. 143–146, doi:10.1130/G37398.1.

Dan, W., Li, X.H., Guo, J., Liu, Y., and Wang, X.C., 2012, Paleoproterozoic evolution of the eastern Alxa Block, westernmost North China: Evidence from in situ zircon U-Pb dating and Hf-O isotopes: Gondwana Research, v. 21, p. 838–864, doi:10.1016/j.gr.2011.09.004.

Dan, W., Li, X.H., Wang, Q., Tang, G.J., and Liu, Y., 2014a, An Early Permian (ca. 280 Ma) silicic igneous province in the Alxa Block, NW China: A magmatic flare-up triggered by a mantle-plume?: Lithos, v. 204, p. 144–158, doi:10.1016/j.lithos.2014.01.018.

Dan, W., Li, X.H., Wang, Q., Wang, X.C., and Liu, Y., 2014b, Neoproterozoic S-type granites in the Alxa Block, westernmost North China and tectonic implications: In situ zircon U-Pb-Hf-O isotopic and geochemical constraints: American Journal of Science, v. 314, p. 110–153, doi:10.2475/01.2014.04.

Dan, W., Li, X.H., Wang, Q., Wang, X.C., Wyman, D.A., and Liu, Y., 2015a, Phanerozoic amalgamation of the Alxa Block and North China craton: Evidence from Paleozoic granitoids, U-Pb geochronology and Sr-Nd-Pb-Hf-O isotope geochemistry: Gondwana Research, doi:10.1016/j.gr.2015.02.011.

Dan, W., Wang, Q., Wang, X.C., Liu, Y., Wyman, D.A., and Liu, Y.S., 2015b, Overlapping Sr-Nd-Hf-O isotopic compositions in Permian mafic enclaves and host granitoids in Alxa Block, NW China: Evidence for crust-mantle interaction and implications for the generation of silicic igneous provinces: Lithos, v. 230, p. 133–145, doi:10.1016/j.lithos.2015.05.016.

Dewey, J.F., and Şengör, A.M.C., 1979, Aegean and surrounding regions: Complex multiplate and continuum tectonics in a convergent zone: Geological Society of America Bulletin, v. 90, no. 1, p. 84–92, doi:10.1130/0016-7606(1979)90<84:AASRCM>2.0.CO;2.

Dhuime, B., Hawkesworth, C., and Cawood, P., 2011, When continents formed: Science, v. 331, no. 6014, p. 154–155, doi:10.1126/science.1201245.

Eizenhöfer, P.R., Zhao, G., Zhang, J., and Sun, M., 2014, Final closure of the Paleo-Asian Ocean along the Solonker Suture Zone: Constraints from geochronological and geochemical data of Permian volcanic and sedimentary rocks: Tectonics, v. 33, p. 441–463, doi:10.1002/2013TC003357.

Eizenhöfer, P.R., Zhao, G.C., Sun, M., Zhang, J., Han, Y.G., and Hou, W.Z., 2015a, Geochronological and Hf isotopic variability of detrital zircons in Paleozoic strata across the accretionary collision zone between the North China craton and Mongolian arcs and tectonic implications: Geological Society of America Bulletin, v. 224–225, p. 240–255, doi:10.1130/B31175.1.

Eizenhöfer, P.R., Zhao, G.C., Zhang, J., Han, Y.G., Hou, W.Z., Liu, D.X., and Wang, B., 2015b, Geochemical characteristics of the Permian basins and their provenances across the Solonker Suture Zone: Assessment of net crustal growth during the closure of the Palaeo-Asian Ocean: Lithos, v. 127, p. 1422–1436, doi:10.1016/j.lithos.2015.03.012.

Feng, J.Y., Xiao, W.J., Windley, B., Han, C.M., Wan, B., Zhang, J.E., Ao, S.J., Zhang, Z.Y., and Lin, L.N., 2013, Field geology, geochronology and geochemistry of mafic-ultramafic rocks from Alxa, China: Implications for Late Permian accretionary tectonics in the southern Altaid: Journal of Asian Earth Sciences, v. 78, p. 114–142, doi:10.1016/j.jseaes.2013.01.020.

Feng, Y.G., Liu, S.W., Lv, Y.J., Tian, W., and Liu, X.M., 2009, Petrogenesis of the late Paleozoic diorites–granitoids in Fengshan area, northern Hebei Province: Constraints from petrochemistry, zircon U-Pb chronology and Hf isotope [in Chinese with English abstract]: Acta Scientiarum Naturalium Universitatis Pekinensis, v. 45, p. 59–70.

Foden, J.D., Elburg, M.A., Turner, S.P., Sandiford, M., O'Callaghan, J., and Mitchell, S., 2002, Granite production in the Delamerian orogen, South Australia: Journal of the Geological Society of London, v. 159, no. 5, p. 557–575, doi:10.1144/0016-764901-099.

Frost, B.R., Barnes, C.G., Collins, W.J., Arculus, R.J., Ellis, D.J., and Frost, C.D., 2001, A geochemical classification for granitic rocks: Journal of Petrology, v. 42, p. 2033–2048, doi:10.1093/petrology/42.11.2033.

Gao, J., Klemd, R., Qian, Q., Zhang, X., Li, J.L., Jiang, T., and Yang, Y.Q., 2011, The collision between the Yili and Tarim blocks of the Southwestern Altaids: Geochemical and age constraints of a leucogranite dike crosscutting the HP-LT metamorphic belt in the Chinese Tianshan Orogen: Tectonophysics, v. 499, p. 118–131, doi:10.1016/j.tecto.2011.01.001.

Geng, Y.S., and Zhou, X.W., 2010, Early Neoproterozoic granite events in Alxa area of Inner Mongolia and their geological significance: Evidence from geochronology [in Chinese with English abstract]: Acta Petrologica et Mineralogica, v. 29, p. 779–795.

Geng, Y.S., and Zhou, X.W., 2011, Characteristics of geochemistry and zircon Hf isotope of the Early Neoproterozoic granite in Alxa area, Inner Mongolia [in Chinese with English abstract]: Yanshi Xuebao, v. 27, p. 897–908.

Geng, Y.S., Wang, X.S., Shen, Q.H., and Wu, C.M., 2002, The discovery of Neoproterozoic Jinningian deformed granites in Alxa area and its significance [in Chinese with English abstract]: Acta Petrologica et Mineralogica, v. 21, p. 412–420.

Gill, J., 1981, Orogenic Andesites and Plate Tectonics: Berlin, Springer-Verlag, 390 p., doi:10.1007/978-3-642-68012-0.

Gong, J.H., Zhang, J.X., Yu, S.Y., Yu, S.Y., Li, H.K., and Hou, K.J., 2012, Ca. 2.5 Ga TTG rocks in the western Alxa Block and their implications: Chinese Science Bulletin, v. 57, p. 4064–4076, doi:10.1007/s11434-012-5315-8.

Gray, C.M., 1984, An isotopic mixing model for the origin of granitic rocks in southeastern Australia: Earth and Planetary Science Letters, v. 70, p. 47–60, doi:10.1016/0012-821X(84)90208-5.

Griffin, W.L., Wang, X., Jackson, S.E., Pearson, N.J., O'Reilly, S.Y., Xu, X.S., and Zhou, X.M., 2002, Zircon chemistry and magma mixing, SE China: In-situ analysis of Hf isotopes, Tonglu and Pingtan igneous complexes: Lithos, v. 61, p. 237–269, doi:10.1016/S0024-4937(02)00082-8.

Han, B.F., He, G.Q., Wang, X.C., and Guo, Z.J., 2011, Late Carboniferous collision between the Tarim and Kazakhstan-Yili terranes in the western segment of the South Tian Shan Orogen, Central Asia, and implications for the Northern Xinjiang, western China: Earth-Science Reviews, v. 109, p. 74–93, doi:10.1016/j.earscirev.2011.09.001.

Han, Y.G., Zhao, G.C., Cawood, P.A., Sun, M., Eizenhöfer, P.R., Hou, W.Z., Zhang, X.R., and Liu, Q., 2016a, Tarim and North China cratons linked to northern Gondwana through switching accretionary tectonics and collisional orogenesis: Geology, v. 44, p. 95–98, doi:10.1130/G37399.1.

Han, Y.G., Zhao, G.C., Sun, M., Eizenhöfer, P.R., Hou, W.Z., Zhang, X.R., Liu, Q., Wang, B., Liu, D.X., and Xu, B., 2016b, Late Paleozoic subduction and collision processes during the amalgamation of the Central Asian Orogenic Belt along the South Tianshan suture zone: Lithos, v. 246–247, p. 1–12, doi:10.1016/j.lithos.2015.12.016.

Hawkesworth, C.J., and Kemp, A.I.S., 2006, Using hafnium and oxygen isotopes in zircons to unravel the record of crustal evolution: Chemical Geology, v. 226, p. 144–162, doi:10.1016/j.chemgeo.2005.09.018.

Hermann, J., and Green, D.H., 2001, Experimental constraints on high pressure melting in subducted crust: Earth and Planetary Science Letters, v. 188, no. 1–2, p. 149–168, doi:10.1016/S0012-821X(01)00321-1.

Hou, W.R., Nie, F.J., Hu, J.M., Liu, Y.F., Xiao, W., Liu, Y., and Zhang, K., 2011, Geochronology and geochemistry of Shadegai granites in Wulashan area, Inner Mongolia and its geological significance [Earth Science Edition]: Journal of Jilin University, v. 41, p. 1914–1927.

Hu, C.S., Li, W.B., Xu, C., Zhong, R.C., Zhu, F., and Qiao, X.Y., 2015, Geochemistry and petrogenesis of Permian granitoids in the northwestern margin of the North China Craton: Insights from the Dongshengmiao pluton, Inner Mongolia: International Geology Review, v. 57, p. 1843–1860, doi:10.1080/00206814.2015.1039087.

Hu, J.M., Gong, W.B., Wu, S.J., Liu, Y., and Liu, S.C., 2014, LA-ICP-MS zircon U-Pb dating of the Langshan Group in the northeast margin of the Alxa block, with tectonic implications: Precambrian Research, v. 255, p. 756–770, doi:10.1016/j.precamres.2014.08.013.

Jackson, S.E., Pearson, N.J., Griffin, W.L., and Belousova, E.A., 2004, The application of laser ablation–inductively coupled plasma–mass spectrometry to in situ U-Pb zircon geochronology: Chemical Geology, v. 211, p. 47–69, doi:10.1016/j.chemgeo.2004.06.017.

Jahn, B., 2004, The Central Asian Orogenic Belt and growth of the continental crust in the Phanerozoic: Geological Society of London, Special Publications, v. 226, p. 73–100, doi:10.1144/GSL.SP.2004.226.01.05.

Jahn, B., Wu, F., and Chen, B., 2000, Massive granitoid generation in Central Asia: Nd isotope evidence and implication for continental growth in the Phanerozoic: Episodes, v. 23, p. 82–92.

Jian, P., Liu, D.Y., Kröner, A., Windley, B.F., Shi, Y.R., Zhang, F.Q., Shi, G.H., Miao, L.C., Zhang, W., Zhang, Q., Zhang, L.Q., and Ren, J.S., 2008, Time scale of an early to mid-Paleozoic orogenic cycle of the long-lived Central Asian Orogenic Belt, Inner Mongolia of China: Implications for continental growth: Lithos, v. 101, p. 233–259, doi:10.1016/j.lithos.2007.07.005.

Jian, P., Liu, D.Y., Kröner, A., Windley, B.F., Shi, Y.R., Zhang, W., Zhang, F.Q., Miao, L.C., Zhang, L.Q., and Tomurhuu, D., 2010, Evolution of a Permian intraoceanic arc-trench system in the Solonker suture zone, Central Asian Orogenic Belt, China and Mongolia: Lithos, v. 118, p. 169–190, doi:10.1016/j.lithos.2010.04.014.

Jiang, N., Liu, Y.S., Zhou, W.G., Yang, J.H., and Zhang, S.Q., 2007, Derivation of Mesozoic adakitic magmas from ancient lower crust in the North China craton: Geochimica et Cosmochimica Acta, v. 71, p. 2591–2608, doi:10.1016/j.gca.2007.02.018.

Kelemen, P.B., Hanghøj, K., and Greene, A.R., 2003, One view of the geochemistry of subduction-related magmatic arcs, with an emphasis on primitive andesite and lower crust: Treatise on geochemistry, v. 3, p. 593–659, doi:10.1016/B0-08-043751-6/03035-8.

Kemp, A.I.S., Hawkesworth, C.J., Foster, G.L., Paterson, B.A., Woodhead, J.D., Hergt, J.M., Gray, C.M., and Whitehouse, M.J., 2007, Magmatic and crustal differentiation history of granitic rocks from Hf-O isotopes in zircon: Science, v. 315, p. 980–983, doi:10.1126/science.1136154.

Kemp, A.I.S., Hawkesworth, C.J., Collins, W.J., Gray, C.M., Blevin, P.L., and EIMF, 2009, Isotopic evidence for rapid continental growth in an extensional accretionary orogen: The Tasmanides, eastern Australia: Earth and Planetary Science Letters, v. 284, p. 455–466, doi:10.1016/j.epsl.2009.05.011.

Khain, E.V., Bibikova, E.V., Salnikova, E.B., Kröner, A., Gibsher, A.S., Didenko, A.N., Degtyarev, K.E., and Fedotova, A.A., 2003, The Palaeo-Asian ocean in the Neoproterozoic and early Palaeozoic: New geochronologic data and palaeotectonic reconstructions: Precambrian Research, v. 122, p. 329–358, doi:10.1016/S0301-9268(02)00218-8.

Klemd, R., John, T., Scherer, E.E., Rondenay, S., and Gao, J., 2011, Changes in dip of subducted slabs at depth: Petrological and geochronological evidence from HP–UHP rocks (Tianshan, NW-China): Earth and Planetary Science Letters, v. 310, p. 9–20, doi:10.1016/j.epsl.2011.07.022.

Li, X.H., Su, L., Song, B., and Liu, D.Y., 2004, SHRIMP U-Pb zircon age of the Jinchuan ultramafic intrusion and its geological significance: Chinese Science Bulletin, v. 49, p. 420–422, doi:10.1007/BF02900329.

Liégeois, J.P., Navez, J., Hertogen, J., and Black, R., 1998, Contrasting origin of post-collisional high-K calc-alkaline and shoshonitic versus alkaline and peralkaline granitoids: The use of sliding normalization: Lithos, v. 45, p. 1–28, doi:10.1016/S0024-4937(98)00023-1.

Lin, L.N., Xiao, W.J., Wan, B., Windley, B.F., Ao, S.J., Han, C.M., Feng, J.Y., Zhang, J.E., and Zhang, Z.Y., 2014, Geochronology and geological evidence for persistence of south-dipping subduction to Late Permian time, Langshan area, Inner Mongolia (China): Significance for termination of accretionary orogenesis in the southern Altaids: American Journal of Science, v. 314, p. 679–703, doi:10.2475/02.2014.08.

Liu, C.S., and Chen, F.R., 1991, Provenance of igneous rocks and binary mixing model [in Chinese with English abstract]: Geological Geochemistry, v. 4, p. 24–32.

Liu, Q., Zhao, G.C., Sun, M., Han, Y.G., Eizenhöfer, P.R., Hou, W.Z., Zhang, X.R., Zhu, Y.L., Wang, B., Liu, D.X., and Xu, B., 2016, Early Paleozoic subduction processes of the Paleo-Asian Ocean: Insights from geochronology and geochemistry of Paleozoic plutons in the Alxa Terrane: Lithos, v. 262, p. 546–560, doi:10.1016/j.lithos.2016.07.041.

Liu, Q., Zhao, G.C., Han, Y.G., Eizenhöfer, P.R., Zhu, Y.L., Hou, W.Z., Zhang, X.R., and Wang, B., 2017, Timing of the final closure of the Paleo-Asian Ocean in the Alxa Terrane: Constraints from geochronology and geochemistry of Late Carboniferous to Permian gabbros and diorites: Lithos, v. 274–275, p. 19–30, doi:10.1016/j.lithos.2016.12.029.

Lu, J.C., Wei, X.Y., Li, Y.H., and Wei, J.S., 2012, Geochemical characteristics of Carboniferous–Permian hydrocarbon source rocks of Xiangtan 9 well in Ejin Banner, western Inner Mongolia [in Chinese with English abstract]: Geological Bulletin of China, v. 31, p. 1628–1638.

Luo, H.L., Wu, T.R., and Li, Y., 2007, Geochemistry and SHRIMP dating of the Kebu massif from Wulatezhongqi, Inner Mongolia: Evidence for the Early Permian underplating beneath the North China Craton [in Chinese with English abstract]: Yanshi Xuebao, v. 23, p. 755–766.

Luo, H.L., Wu, T.R., Zhao, L., He, Y.K., and Xu, J., 2013, Geochemical characteristics of Bayinzhurihe pluton and its tectonic significance, Bayan Obo [in Chinese with English abstract]: Inner Mongolia: Geological Journal of China Universities, v. 19, p. 123–132.

Luo, Z.K., Li, J.J., and Guan, K., 2004, SHRIMP zircon U–Pb age of the granite at Baizhangzi gold field in Lingyuan, Liaoning Province [in Chinese with English abstract]: Geological Survey and Research, v. 27, p. 82–85.

Maniar, P.D., and Piccoli, P.M., 1989, Tectonic discrimination of granitoids: Geological Society of America Bulletin, v. 101, p. 635–643, doi:10.1130/0016-7606(1989)101<0635:TDOG>2.3.CO;2.

McDonough, W.F., and Sun, S.S., 1995, The composition of the Earth: Chemical Geology, v. 120, p. 223–253, doi:10.1016/0009-2541(94)00140-4.

Miao, L., Zhang, F., Fan, W.M., and Liu, D., 2007, Phanerozoic evolution of the Inner Mongolia–Daxinganling orogenic belt in North China: Constraints from geochronology of ophiolites and associated formations: Geological Society of London, Special Publications, v. 280, p. 223–237, doi:10.1144/SP280.11.

Mo, N., Guo, L., Tong, Y., Wang, T., Liu, J., and Li, J.B., 2014, Geochronology, geochemistry, Hf isotope of Xiaojinggou pluton in the northern margin of North China Craton and its tectonic implications [in Chinese with English abstract]: Beijing Da Xue Xue Bao, Zi Ran Ke Xue Bao, v. 50, p. 1021–1034.

Moyen, J.F., Martin, H., and Jayananda, M., 2001, Multi-element geochemical modelling of crust–mantle interactions during late-Archaean crustal growth: The Closepet granite (South India): Precambrian Research, v. 112, p. 87–105, doi:10.1016/S0301-9268(01)00171-1.

Nandedkar, R.H., Ulmer, P., and Müntener, O., 2014, Fractional crystallization of primitive, hydrous arc magmas: an experimental study at 0.7 GPa: Contributions to Mineralogy and Petrology, v. 167, no. 6, doi:10.1007/s00410-014-1015-5.

Patiño Douce, A.E.P., 1995, Experimental generation of hybrid silicic melts by reaction of high-Al basalt with metamorphic rocks: Journal of Geophysical Research, v. 100, p. 15623–15639, doi:10.1029/94JB03376.

Patiño Douce, A.E.P., 1999, What do experiments tell us about the relative contributions of crust and mantle to the origin of granitic magmas?: Geological Society of London, Special Publications, v. 168, p. 55–75, doi:10.1144/GSL.SP.1999.168.01.05.

Pearce, J.A., 1983, Role of the sub-continental lithosphere in magma genesis at active continental margins, *in* Hawkesworth, C.J., and Norry, M.J., eds., Continental Basalts and Mantle Xenoliths: Shiva, Nantwich, p. 230–249.

Peccerillo, A., and Taylor, S.R., 1976, Geochemistry of Eocene calc-alkaline volcanic rocks from the Kastamonu area, northern Turkey: Contributions to Mineralogy and Petrology, v. 58, p. 63–81, doi:10.1007/BF00384745.

Peng, R.M., Zhai, Y.S., Wang, J.P., Chen, X.F., Liu, Q., Lv, J.Y., Shi, Y.X., Wang, G., Li, S.B., Wang, L.G., Ma, Y.T., and Zhang, P., 2010, Discovery of Neoproterozoic acid volcanic rock in the western section of Langshan, Inner Mongolia, and its geological significance [in Chinese]: Chinese Science Bulletin, v. 55, p. 2611–2620, doi:10.1360/972010-266.

Peng, R.M., Zhai, Y.S., Li, C.S., and Ripley, E.M., 2013, The Erbutu Ni-Cu deposit in the Central Asian Orogenic Belt: A Permian magmatic sulfide deposit related to boninitic magmatism in an arc setting: Economic Geology and the Bulletin of the Society of Economic Geologists, v. 108, p. 1879–1888, doi:10.2113/econgeo.108.8.1879.

Pi, Q.H., Liu, C.Z., Chen, Y.L., Li, Q.Q., and Li, D.P., 2010, Formation epoch and genesis of intrusive rocks in Huogeqi ore field of Inner Mongolia and their relationship with copper mineralization [in Chinese with English abstract]: Mineralium Deposita, v. 29, p. 437–451.

Ran, H., Zhang, W.J., and Liu, Z.B., 2012, Geochemical characteristics and LA-ICP-MS zircon U-Pb dating of the Late Permian monzogranite in Hanggale, Alxa Right Banner, Inner Mongolia [in Chinese with English abstract]: Geological Bulletin of China, v. 31, p. 1565–1575.

Reubi, O., and Blundy, J., 2009, A dearth of intermediate melts at subduction zone volcanoes and the petrogenesis of arc andesites: Nature, v. 461, p. 1269–1273, doi:10.1038/nature08510.

Roberts, N.M.W., Slagstad, T., Parrish, R.R., Norry, M.J., Marker, M., and Horstwood, M.S.A., 2013, Sedimentary recycling in arc magmas: Geochemical and U-Pb-Hf-O constraints on the Mesoproterozoic Suldal Arc, SW Norway: Contributions to Mineralogy and Petrology, v. 165, p. 507–523, doi:10.1007/s00410-012-0820-y.

Scherer, E., Munker, C., and Mezger, K., 2001, Calibration of the Lutetium-Hafnium clock: Science, v. 293, p. 683–687, doi:10.1126/science.1061372.

Schulmann, K., and Paterson, S., 2011, Geodynamics: Asian continental growth: Nature Geoscience, v. 4, p. 827–829, doi:10.1038/ngeo1339.

Şengör, A.M.C., Natal'in, B.A., and Burtman, V.S., 1993, Evolution of the Altaid tectonic collage and Palaeozoic crustal growth in Eurasia: Nature, v. 364, p. 299–307, doi:10.1038/364299a0.

Shi, X.J., Tong, Y., Wang, T., Zhang, J.J., Zhang, Z.C., Zhang, L., Guo, L., Zeng, T., and Geng, J.Z., 2012, LA-ICP-MS zircon U-Pb age and geochemistry of the Early Permian Halinudeng granite in northern Alxa area, western Inner Mongolia [in Chinese with English abstract]: Geological Bulletin of China, v. 31, p. 662–670.

Shi, X.J., Wang, T., Zhang, L., Castro, A., Xiao, X.C., Tong, Y., Zhang, J.J., Guo, L., and Yang, Q.D., 2014a, Timing, petrogenesis and tectonic setting of the Late Paleozoic gabbro-granodiorite-granite intrusions in the Shalazhashan of northern Alxa: Constraints on the southernmost boundary of the Central Asian Orogenic Belt: Lithos, v. 208–209, p. 158–177, doi:10.1016/j.lithos.2014.08.024.

Shi, X.J., Zhang, L., Wang, T., Xiao, X.C., Tong, Y., Zhang, J.J., Geng, J.Z., and Ye, K., 2014b, Geochronology and geochemistry of the intermediate-acid intrusive rocks from Zongnaishan area in northern Alxa, Inner Mongolia, and their tectonic implications [in Chinese with English abstract]: Acta Petrologica et Mineralogica, v. 33, p. 989–1007.

Smits, R.G., Collins, W.J., Hand, M., Dutch, R., and Rayne, J., 2014, A Proterozoic Wilson cycle identified by Hf isotopes in central Australia: Implications for the assembly of Proterozoic Australia and Rodinia: Geology, v. 42, p. 231–234, doi:10.1130/G35112.1.

Sylvester, P.J., 1998, Post-collisional strongly peraluminous granites: Lithos, v. 45, p. 29–44, doi:10.1016/S0024-4937(98)00024-3.

Tang, Q., Li, C., Zhang, M.M., Ripley, E., and Wang, Q.L., 2014, Detrital zircon constraint on the timing of amalgamation between Alxa and Ordos, with exploration implications for Jinchuan-type Ni-Cu ore deposit in China: Precambrian Research, v. 255, p. 748–755, doi:10.1016/j.precamres.2014.08.015.

Tepley, F.J., Davidson, J.P., Tilling, R.I., and Arth, J.G., 2000, Magma mixing, recharge and eruption histories recorded in plagioclase phenocrysts from El Chichon Volcano, Mexico: Journal of Petrology, v. 41, p. 1397–1411, doi:10.1093/petrology/41.9.1397.

Tian, W., Chen, B., Liu, C.Q., and Zhang, H.F., 2007, Zircon U-Pb age and Hf isotopic composition of the Xiaozhangjiakou ultramafic pluton in northern Hebei [in Chinese with English abstract]: Yanshi Xuebao, v. 23, p. 583–590.

Vervoort, J.D., and Blichert-Toft, J., 1999, Evolution of the depleted mantle: Hf isotope evidence from juvenile rocks through time: Geochimica et Cosmochimica Acta, v. 63, p. 533–556, doi:10.1016/S0016-7037(98)00274-9.

Wang, F., Chen, F.K., Hou, Z.H., Peng, P., and Zhai, M.G., 2009, Zircon ages and Sr-Nd-Hf isotopic composition of late Paleozoic granitoids in the Chongli-Chicheng area, northern margin of the North China Block [in Chinese with English abstract]: Yanshi Xuebao, v. 25, p. 3057–3074.

Wang, T.Y., Wang, S.Z., and Wang, J.R., 1994, The Formation and Evolution of Paleozoic Continental Crust in Alxa Region: Lanzhou University Press, Lanzhou, 213 p. (in Chinese).

Wang, Z.J., Xu, W.L., Pei, F.P., Wang, Z.W., Li, Y., and Cao, H.H., 2015a, Geochronology and geochemistry of middle Permian–Middle Triassic intrusive rocks from central-eastern Jilin Province, NE China: Constrains on the tectonic evolution of the eastern segment of the Paleo-Asian Ocean: Lithos, v. 238, p. 13–25, doi:10.1016/j.lithos.2015.09.019.

Wang, Z.Z., Han, B.F., Feng, L.X., and Liu, B., 2015b, Geochronology, geochemistry and origins of the Paleozoic–Triassic plutons in the Langshan area, western Inner Mongolia, China: Journal of Asian Earth Sciences, v. 97, p. 337–351, doi:10.1016/j.jseaes.2014.08.005.

Watson, E.B., and Harrison, T.M., 1983, Zircon saturation revisited: Temperature and composition effects in a variety of crustal magma types: Earth and Planetary Science Letters, v. 64, no. 2, p. 295–304, doi:10.1016/0012-821X(83)90211-X.

Whalen, J.B., Currie, K.L., and Chappell, B.W., 1987, A-type granites: Geochemical characteristics, discrimination and petrogenesis: Contributions to Mineralogy and Petrology, v. 95, p. 407–419, doi:10.1007/BF00402202.

Wiedenbeck, M., Alle, P., Corfu, F., Griffin, W.L., Meier, M., Von Quadt, A., Roddick, J.C., and Spiegel, W., 1995, Three natural zircon standards for U-Th-Pb, Lu-Hf, trace element and REE analyses: Geostandards Newsletter, v. 19, p. 1–23, doi:10.1111/j.1751-908X.1995.tb00147.x.

Wilhem, C., Windley, B.F., and Stampfli, G.M., 2012, The Altaids of Central Asia: A tectonic and evolutionary innovative review: Earth-Science Reviews, v. 113, p. 303–341, doi:10.1016/j.earscirev.2012.04.001.

Windley, B.F., Alexeiev, D., Xiao, W.J., Kröner, A., and Badarch, G., 2007, Tectonic models for accretion of the Central Asian Orogenic Belt: Journal of the Geological Society of London, v. 164, p. 31–47, doi:10.1144/0016-76492006-022.

Wu, S.J., Hu, J.M., Ren, M.H., Gong, W.B., Liu, Y., and Yan, J.Y., 2014, Petrography and zircon U-Pb isotopic study of the Bayanwulashan Complex: Constraints on the Paleoproterozoic evolution of the Alxa Block, westernmost North China Craton: Journal of Asian Earth Sciences, v. 94, p. 226–239, doi:10.1016/j.jseaes.2014.05.011.

Wu, T.R., He, G.Q., and Zhang, C., 1998, On Paleozoic tectonics in the Alxa region: Acta Geologica Sinica, v. 72, p. 256–263.

Wu, Y.F., Zeng, J.N., Cao, J.J., Wu, Z.Q., Chen, J.H., Zhou, S.D., Lu, S.F., and Li, X.F., 2013, Zircon U-Pb ages and Hf isotope of Hercynian intrusion in Dongshengmiao, Inner Mongolia [in Chinese with English abstract]: Geological Science and Technology Information, v. 32, p. 22–30.

Xiao, W.J., Windley, B.F., Hao, J., and Zhai, M.G., 2003, Accretion leading to collision and the Permian Solonker suture, Inner Mongolia, China: Termination of the Central Asian orogenic belt: Tectonics, v. 22, doi:10.1029/2002TC001484.

Xiao, W.J., Windley, B.F., Huang, B.C., Han, C.M., Yuan, C., Chen, H.L., Sun, M., Sun, S., and Li, J.L., 2009, End-Permian to mid-Triassic termination of the accretionary processes of the southern Altaids: Implications for the geodynamic evolution, Phanerozoic continental growth, and metallogeny of Central Asia: International Journal of Earth Sciences, v. 98, p. 1189–1217, doi:10.1007/s00531-008-0407-z.

Xiao, W.J., Windley, B.F., Allen, M.B., and Han, C.M., 2013, Paleozoic multiple accretionary and collisional tectonics of the Chinese Tianshan orogenic collage: Gondwana Research, v. 23, p. 1316–1341, doi:10.1016/j.gr.2012.01.012.

Xiao, W.J., Windley, B., Sun, S., Li, J.L., Huang, B.C., Han, C.M., Yuan, C., Sun, M., and Chen, H.L., 2015, A tale of amalgamation of three Permo–Triassic collage systems in Central Asia: Oroclines, sutures, and terminal accretion: Annual Review of Earth and Planetary Sciences, v. 43, p. 477–507, doi:10.1146/annurev-earth-060614-105254.

Xie, L., Yin, H.Q., Zhou, H.R., and Zhang, W.J., 2014, Permian radiolarians from the Engeerwusu suture zone in Alxa area of Inner Mongolia and its geological significance [in Chinese with English abstract]: Geological Bulletin of China, v. 33, p. 691–697.

Xu, B., Charvet, J., Chen, Y., Zhao, P., and Shi, G.Z., 2013, Middle Paleozoic convergent orogenic belts in western Inner Mongolia (China): Framework, kinematics, geochronology and implications for tectonic evolution of the Central Asian Orogenic Belt: Gondwana Research, v. 23, p. 1342–1364, doi:10.1016/j.gr.2012.05.015.

Yang, J.H., Wu, F.Y., Wilde, S.A., Belousova, E., and Griffin, W.L., 2008, Mesozoic decratonization of the North China block: Geology, v. 36, p. 467–470, doi:10.1130/G24518A.1.

Yang, Q.D., Zhang, L., Wan, T., Shi, X.J., Zhang, J.J., Tong, Y., Guo, L., and Geng, J.Z., 2014, Geochemistry and LA-ICP-MS zircon U-Pb age of Late Carboniferous Shalazhashan pluton on the northern margin of the Alxa Block, Inner Mongolia and their implications [in Chinese with English abstract]: Geological Bulletin of China, v. 33, p. 776–787.

Yu, J.H., Zhou, X.M., Zhao, L., Jiang, S.Y., Wang, L.J., and Ling, H.F., 2005, Mantle-crust interaction generating the Wuping granites: Evidence from Sr-Nd-Hf-U-Pb isotopes [in Chinese with English abstract]: Yanshi Xuebao, v. 21, p. 651–664.

Zhang, J.X., Gong, J.H., Yu, S.Y., Li, H.K., and Hou, K.J., 2013, Neoarchean–Paleoproterozoic multiple tectonothermal events in the western Alxa block, North China Craton and their geological implication: Evidence from zircon U-Pb ages and Hf isotopic composition: Precambrian Research, v. 235, p. 36–57, doi:10.1016/j.precamres.2013.05.002.

Zhang, L., Shi, X.J., Zhang, J.J., Yang, Q.D., Tong, Y., and Wang, T., 2013, LA-ICP-MS zircon U-Pb age and geochemical characteristics of the Taohaotuoxiquan gabbro in northern Alxa, Inner Mongolia [in Chinese with English abstract]: Geological Bulletin of China, v. 32, p. 1536–1547.

Zhang, S.H., Zhao, Y., Song, B., Yang, Z.Y., Hu, J.M., and Wu, H., 2007, Carboniferous granitic plutons from the northern margin of the North China block: Implications for a late Palaeozoic active continental margin: Journal of the Geological Society of London, v. 164, p. 451–463, doi:10.1144/0016-76492005-190.

Zhang, S.H., Zhao, Y., Kröner, A., Liu, X.M., Xie, X.M., Xie, L.W., and Chen, F.K., 2009a, Early Permian plutons from the northern North China Block: Constraints on continental arc evolution and convergent margin magmatism related to the Central Asian Orogenic Belt: International Journal of Earth Sciences, v. 98, p. 1441–1467, doi:10.1007/s00531-008-0368-2.

Zhang, S.H., Zhao, Y., Liu, X.C., Liu, D.Y., Chen, F.K., Xie, L.W., and Chen, H.H., 2009b, Late Paleozoic to Early Mesozoic mafic-ultramafic complexes from the northern North China Block: Constraints on the composition and evolution of the lithospheric mantle: Lithos, v. 110, p. 229–246, doi:10.1016/j.lithos.2009.01.008.

Zhang, S.H., Zhao, Y., Song, B., Hu, J.M., Liu, S.W., Yang, Y.H., Chen, F.K., Liu, X.M., and Liu, J., 2009c, Contrasting Late Carboniferous and Late Permian–Middle Triassic intrusive suites from the northern margin of the North China craton: Geochronology, petrogenesis, and tectonic implications: Geological Society of America Bulletin, v. 121, p. 181–200, doi:10.1130/B26157.1.

Zhang, W., Jian, P., Liu, D.Y., and Hou, K.J., 2010, Geochemistry, geochronology and Hf isotopic compositions of Triassic granodiorite-diorite and shoshonite from the Damaoqi area, central Inner Mongolia, China [in Chinese with English abstract]: Geological Bulletin of China, v. 29, p. 821–832.

Zhang, W., Wu, T.R., Feng, J.C., Zheng, R.G., and He, Y.K., 2013, Time constraints for the closing of the Paleo-Asian Ocean in the Northern Alxa Region: Evidence from Wuliji granites: Science China Earth Sciences, v. 56, p. 153–164, doi:10.1007/s11430-012-4435-y.

Zhang, X.H., Miao, Q., Zhang, H.F., Zhai, M.G., Yang, Y.H., and Hu, Z.C., 2011, Mafic and felsic magma interaction during the construction of high-K calc-alkaline plutons within a metacratonic passive margin: The Early Permian Guyang batholith from the northern North China Craton: Lithos, v. 125, p. 569–591, doi:10.1016/j.lithos.2011.03.008.

Zhang, X.H., Gao, Y.L., Wang, Z.J., Liu, H., and Ma, Y.G., 2012a, Carboniferous appinitic intrusions from the northern North China craton: Geochemistry, petrogenesis, and tectonic implications: Journal of the Geological Society of London, v. 169, p. 337–351, doi:10.1144/0016-76492011-062.

Zhang, X.H., Xue, F.H., Yuan, L.L., Ma, Y.G., and Wilde, S.A., 2012b, Late Permian appinite-granite complex from northwestern Liaoning, North China Craton: Petrogenesis and tectonic implications: Lithos, v. 155, p. 201–217, doi:10.1016/j.lithos.2012.09.002.

Zhang, X.R., Zhao, G.C., Eizenhöfer, P.R., Sun, M., Han, Y.G., Hou, W.Z., Liu, D.X., Wang, B., Liu, Q., and Xu, B., 2015a, Latest Carboniferous closure of the Junggar Ocean constrained by geochemical and zircon U-Pb-Hf isotopic data of granitic gneisses from the Central Tianshan block, NW China: Lithos, v. 238, p. 26–36, doi:10.1016/j.lithos.2015.09.012.

Zhang, X.R., Zhao, G.C., Eizenhöfer, P.R., Sun, M., Han, Y.G., Hou, W.Z., Liu, D.X., Wang, B., Liu, Q., and Xu, B., 2015b, Paleozoic magmatism and metamorphism in the Central Tianshan block revealed by U-Pb and Lu-Hf isotope studies of detrital zircons from the South Tianshan belt, NW China: Lithos, v. 233, p. 193–208, doi:10.1016/j.lithos.2015.06.002.

Zhang, X.R., Zhao, G.C., Sun, M., Eizenhöfer, P.R., Han, Y.G., Hou, W.Z., Liu, D.X., Wang, B., Liu, Q., and Xu, B., 2016a, Tectonic evolution from subduction to arc-continent collision of the Junggar ocean: Constraints from U-Pb dating and Hf isotopes of detrital zircons from the North Tianshan belt, NW China: Geological Society of America Bulletin, v. 128, p. 644–660, doi:10.1130/B31230.1.

Zhang, X.R., Zhao, G.C., Eizenhöfer, P.R., Sun, M., Han, Y.G., Hou, W.Z., Liu, D.X., Wang, B., Liu, Q., Xu, B., and Zhu, C.Y.L, 2016b, Tectonic transition from Late Carboniferous subduction to Early Permian post-collisional extension in the Eastern Tianshan, NW China: Insights from geochronology and geochemistry of mafic-intermediate intrusions: Lithos, v. 256–257, p. 269–281, doi:10.1016/j.lithos.2016.04.006.

Zhang, Y.B., Wu, F.Y., Wilde, S.A., Zhai, M.G., Lu, X.P., and Sun, D.Y., 2004, Zircon U-Pb ages and tectonic implications of 'Early Paleozoic' granitoids at Yanbian, Jilin Province, northeast China: The Island Arc, v. 13, p. 484–505, doi:10.1111/j.1440-1738.2004.00442.x.

Zhao, L., Wu, T.R., and Luo, H.L., 2011, SHRIMP U-Pb dating, geochemistry and tectonic implications of the Beiqigetao gabbros in Urad Zhongqi area, Inner Mongolia [in Chinese with English abstract]: Yanshi Xuebao, v. 27, p. 3071–3082.

Zhao, Y., Sun, Y., Yan, J., and Diwu, C., 2015, The Archean–Paleoproterozoic crustal evolution in the Dunhuang region, NW China: Constraints from zircon U-Pb geochronology and in situ Hf isotopes: Precambrian Research, v. 271, p. 83–97, doi:10.1016/j.precamres.2015.10.002.

Zheng, R.G., Wu, T.R., Zhang, W., Xu, C., Meng, Q.P., and Zhang, Z.Y., 2014, Late Paleozoic subduction system in the northern margin of the Alxa block, Altaids: Geochronological and geochemical evidences from ophiolites: Gondwana Research, v. 25, p. 842–858, doi:10.1016/j.gr.2013.05.011.

Zhou, X.M., and Li, W.X., 2000, Origin of Late Mesozoic igneous rocks in Southeastern China: Implications for lithosphere subduction and underplating of mafic magmas: Tectonophysics, v. 326, p. 269–287, doi:10.1016/S0040-1951(00)00120-7.

MANUSCRIPT RECEIVED 7 JANUARY 2017
REVISED MANUSCRIPT RECEIVED 3 APRIL 2017
MANUSCRIPT ACCEPTED 4 MAY 2017

Printed in the USA